

2010

In-plane thermal conductivity modeling of carbon filled liquid crystal polymer based resins

Tayloria N. G. Adams
Michigan Technological University

Follow this and additional works at: <https://digitalcommons.mtu.edu/etds>


 Part of the [Chemical Engineering Commons](#)

Copyright 2010 Tayloria N. G. Adams

Recommended Citation

Adams, Tayloria N. G., "In-plane thermal conductivity modeling of carbon filled liquid crystal polymer based resins", Master's Thesis, Michigan Technological University, 2010.
<https://doi.org/10.37099/mtu.dc.etds/9>

Follow this and additional works at: <https://digitalcommons.mtu.edu/etds>

 Part of the [Chemical Engineering Commons](#)

In-Plane Thermal Conductivity Modeling of Carbon Filled Liquid Crystal Polymer Based Resins

By

Tayloria N. G. Adams

A THESIS

Submitted in partial fulfillment of the requirements

For the degree of

Master of Science

(Chemical Engineering)

Michigan Technological University

2010

This thesis, **“In-Plane Thermal Conductivity Modeling of Carbon Filled Liquid Crystal Polymer Based Resins,”** is hereby approved in partial fulfillment of the requirements for the degree of MASTER OF SCIENCE in the field of Chemical Engineering.

Department – Chemical Engineering

Signatures:

Thesis Co-Advisor

Dr. Julia King

Thesis Co-Advisor

Dr. Tamara Olson

Department Chair

Dr. S. Komar Kawatra

Date: _____

ABSTRACT

“In-Plane Thermal Conductivity Modeling of Carbon Filler Liquid Crystal Polymer Based Resins”

Adding conductive carbon fillers to insulating thermoplastic resins increases composite electrical and thermal conductivity. Often, as much of a single type of carbon filler is added to achieve the desired conductivity, while still allowing the material to be molded into a bipolar plate for a fuel cell. In this study, varying amounts of three different carbons (carbon black, synthetic graphite particles, and carbon fiber) were added to Vectra A950RX Liquid Crystal Polymer. The in-plane thermal conductivity of the resulting single filler composites were tested. The results showed that adding synthetic graphite particles caused the largest increase in the in-plane thermal conductivity of the composite.

The composites were modeled using ellipsoidal inclusion problems to predict the effective in-plane thermal conductivities at varying volume fractions with only physical property data of constituents. The synthetic graphite and carbon black were modeled using the average field approximation with ellipsoidal inclusions and the model showed good agreement with the experimental data. The carbon fiber polymer composite was modeled using an assemblage of coated ellipsoids and the model showed good agreement with the experimental data.

ACKNOWLEDGEMENTS

First and foremost I would like to thank my advisors, Dr. Julia King and Dr. Tamara Olson, along with my committee member Dr. Jason Keith. Your knowledge, insight, and guidance throughout my project has been very helpful.

I would like to thank the Department of Energy (Award Number DE-FG36-08GO88104), the King-Chavez-Parks State of Michigan Fellowship, and the National GEM Consortium for providing funding for this work.

I would like to thank my friends Carnell Hunter, Renee Oats, and Kabongo Ngandu. Your advice and encouragement has really helped me. I would like to thank my sisters Dawn Adams and Monica Sprowls, you all have been a great support system. I would like to thank my mother, Gloria Adams, you're my biggest cheerleader and you have always encouraged me to strive, work hard, and do more. I would like to thank my grandmother, Linda Adams, for always knowing her namesake would do something special. I would like to thank my father, Jonah Adams; he is gone but never forgotten.

Finally, I would like to give the biggest thank you to my daughter, Aiyanna Adams. When I told her we would be leaving our family in Virginia and moving all the way to Upper Michigan she was like "Ok!" She has been my best friend and my biggest inspiration, I love you!

TABLE OF CONTENTS

Abstract.....	iii
Acknowledgements	iv
List of Figures.....	ix
List of Tables	xi
Table of Nomenclature	xii
Chapter 1: Introduction	1
1.1 Introduction and Motivation	1
1.2 Objectives	4
1.3 References.....	5
Chapter 2: Background.....	8
2.1 Fuel Cells	8
2.1.1 Proton Exchange Membrane Fuel Cells and Bipolar Plates	11
2.2 Thermal Conductivity	14
2.3 Thermal Conductivity Modeling.....	16
2.3.1 Inclusion Problem	19
2.3.2 Polarizability of a Spherical and Elliptical Inclusion	21
2.3.3 Maxwell's Garnett's Approximation	23
2.3.4 Effective Medium Approximation	25
2.3.5 Average Field Approximation	27
2.3.6 Assemblage of Neutral Inclusions	31
2.3.7 Nielsen's Model	35
2.4 References.....	40

Chapter 3: Materials.....	44
3.1 Materials	44
3.2 Matrix Material	44
3.2.1 Vectra A950RX Liquid Crystal Polymer.....	44
3.3 Filler Materials.....	45
3.3.1 Carbon Black	45
3.3.2 Synthetic Graphite	47
3.3.3 PAN-Based Carbon Fiber	49
3.3.4 Formulation Naming Convention	54
3.4 References.....	56
Chapter 4: Fabrication and Experimental Methods	58
4.1 Fabrication Methods	58
4.1.1 Drying	58
4.1.2 Extrusion	59
4.1.3 Injection Molding.....	61
4.2 Experimental Test Methods	64
4.2.1 Hot Disk Specific Heat	64
4.2.2 Hot Disk Thermal Analyzer for Transverse and Longitudinal Thermal Conductivity	63
4.2.3 Density	67
4.2.4 Solvent Digestion.....	68
4.2.5 Filler Length and Aspect Ratio	70
4.2.6 Determination of Particle Orientation in the Composite	73

4.2.6.1 Sample Preparation.....	75
4.2.6.2 Polishing	76
4.2.6.3 Optical Imaging Methods	79
4.3 References.....	81
Chapter 5: In-Plane Thermal Conductivity Modeling.....	83
5.1 In-Plane Thermal Conductivity Modeling.....	83
5.2 Modeling Theory	83
5.2.1 Synthetic Graphite and Carbon Black Models.....	84
5.2.2 Carbon Fiber Model	89
5.3 Results.....	93
5.3.1 Filler Length, Aspect Ratio, and Orientation Results	93
5.3.2 In-Plane Thermal Conductivity Experimental Results	95
5.3.3 In-Plane Thermal Conductivity Modeling Results	97
5.3.3.1 Synthetic Graphite Model	97
5.3.3.2 Carbon Black Model	99
5.3.3.3 Carbon Fiber Model	101
5.4 Conclusions.....	103
5.5 References.....	105
Chapter 6: Summary, Conclusion, and Future Work.....	107
6.1 Summary	107
6.2 Conclusion	108
6.3 Future Work	109
6.4 References.....	111
Appendix A: Extruder Screw Design.....	112

Appendix B: Mathematica Code for Synthetic Graphite and	
Carbon Black Model.....	113
Appendix C: Mathematica Code for Carbon Fiber.....	115
Appendix D: Permission Letter	119

LIST OF FIGURES

Figure 2.1-1: Diagram of a Fuel Cell [2]	9
Figure 2.1-2: Schematic of a Proton Exchange Membrane Fuel Cell	12
Figure 2.2-1: Two-Dimensional Array of Atoms Connected by Springs [15]	15
Figure 2.3-1: Neutral Spherical Inclusion.....	31
Figure 3.2-1: Chemical Structure for Vectra A950RX LCP [3].....	45
Figure 3.3-1: Carbon Black [3]	47
Figure 3.3-2: Thermocarb TC-300 Synthetic Graphite ESEM Image at 200X Magnification [3]	49
Figure 3.3-3: Structural Formula of Polyacrylonitrile (PAN) [12].....	50
Figure 3.3-4: Process Steps of Carbon Fiber Production from Polyacrylonitrile [12] ...	51
Figure 3.3-5: Fortafil 243 Carbon Fiber ESEM Image at 250X Magnification [3].....	53
Figure 3.3-6: Fortafil 243 Carbon Fiber ESEM Image at 1000X Magnification [3].....	53
Figure 4.1-1: Bry Air Dryer System	58
Figure 4.1-2: American Leistritz Extruder with 27 mm Twin Screw	59
Figure 4.1-3: AccuRate Flexwall Feeder	60
Figure 4.1-4: AccuRate Conisteel Feeder	60
Figure 4.1-5: Water Bath and Pelletizer	61
Figure 4.1-6: Niigata Model NE85UA4 Injection Molding Machine	62
Figure 4.1-7: Four-Cavity Mold	63
Figure 4.2-1: Hot Disk Thermal Constants Analyser	65
Figure 4.2-2: Diagram of Samples and Sensor	66
Figure 4.2-3: Solvent Digestion Filtration Apparatus.....	72

Figure 4.2-4: Filler Dispersion Apparatus	73
Figure 4.2-5: Microscope Setup Used for Filler Length and Aspect Ratio	74
Figure 4.2-6: Ground Oval-Shape Epoxy Pucks.....	76
Figure 4.2-7: Prepared Polymer Puck	77
Figure 4.2-8: Image of Cut Off Saw Used to Cut Epoxy Puck into Thin Sections	77
Figure 4.2-9: Thin Sections of Composite Samples Ready for Polishing	78
Figure 4.2-10: Buehler Ecomet 4 Grinder/Polisher	78
Figure 4.2-11: Olympus BX60 Microscope.....	80
Figure 5.2-1: Diagram of Uncoated Ellipsoid.....	88
Figure 5.2-2: Diagram of Ellipsoidal Inclusion Problem.....	90
Figure 5.2-3: Diagram of Coated Ellipsoid.....	91
Figure 5.3-1: In-Plane Orientation of 40 wt% SG in Vectra Injection Molded Disk at a Magnification of 200X	94
Figure 5.3-2: In-Plane Orientation of 20 wt% CF in Vectra Injection Modeled Disk at a Magnification of 200X	94
Figure 5.3-3: Modeling Results of In-Plane Thermal Conductivity of SG/Vectra Composites.....	98
Figure 5.3-4: Modeling Results of In-Plane Thermal Conductivity of CB/Vectra Composites.....	100
Figure 5.3-5: Modeling Results of In-Plane Thermal Conductivity of CF/Vectra Composites	103

LIST OF TABLES

Table 1.1-1: Summary of the Five Main Fuel Cells [1-5]	2
Table 1.1-2: Thermal Conductivity for Common Materials [10]	3
Table 2.1-1: Detailed Summary of the Five Main of Fuel Cells [1-5]	11
Table 2.3-1: Shape Factor ‘A’ for Common Filler Types [11].....	37
Table 2.3-2: Maximum Packing Fraction of Selected Fillers [11]	38
Table 3.2-1: Properties of Ticona’s Vectra A950RX LCP [3]	45
Table 3.3-1: Properties of Akzo Nobel Ketjenblack EC-600 JD [5]	47
Table 3.3-2: Properties of Thermocarb TC-300 Synthetic Graphite [10].....	48
Table 3.3-3: Properties of Toho Tenax America’s Fortafil 243 Carbon Fiber [14]	52
Table 3.3-4: Single Filler Loading Levels	55
Table 5.3-1: Single Filler Loading Levels in Vectra A950RX and Experimental and Model In-Plane Thermal Conductivity	96

NOMENCLATURE

a_i	Constant from the assemblage of neutral inclusion model (Eq. 2-42)
a^*	Constant from the assemblage of neutral inclusion model (Eq. 2-44)
A	Nielsen model equation parameter
AR	Aspect ratio of a material
b_i	Constant from the assemblage of neutral inclusion model (Eq. 2-42)
b^*	Constant from the assemblage of neutral inclusion model (Eq. 2-44)
B	Nielsen model equation parameter
c	Volumetric heat capacity ($J/m^3 \cdot K$)
C	Trendline equation parameter
\hat{C}_p	Heat capacity of a component ($J/Kg \cdot K$)
d_i	Depolarization factors of an ellipsoid
d_{ci}	Depolarization factor of a core ellipsoid
d_{ei}	Depolarization factor of an exterior ellipsoid
D	Trendline equation parameter
D	Sample diameter (cm)
D	Depolarization tensor of an inclusion (Eq. 5-16)
$\underline{\underline{D}}_c$	Depolarization tensor of a core ellipsoid
$\underline{\underline{D}}_e$	Depolarization of an exterior ellipsoid
f_i	Volume fraction of a component
$F(\tau)$	Dimensionless time dependent function
I	Identity matrix
k	Thermal conductivity ($W/m \cdot K$)

k_i	Thermal conductivity of a component (W/m·K)
\underline{k}_i	Thermal conductivity tensor of a component (W/m·K)
\underline{k}_m	Thermal conductivity tensor of the matrix material (W/m·K)
k^*	Effective thermal conductivity (W/m·K)
\underline{k}^*	Effective thermal conductivity tensor (W/m·K)
k_{in}	In-plane thermal conductivity (W/m·K)
$k_{through}$	Through-plane thermal conductivity (W/m·K)
k_i^β	Principle thermal conductivity of phase i of a material (W/m·K)
$k_i[i, i]$	Diagonal matrix entry of the thermal conductivity of a material (W/m·K)
$k_*[i, i]$	Diagonal matrix entry of the effective thermal conductivity (W/m·K)
l	Ring number
l_i	Semi-axis of an isotropic ellipsoid
l'_{ci}	Semi-axis of a core anisotropic ellipsoid
l'_{ei}	Semi-axis of an exterior anisotropic ellipsoid
L_i^β	Depolarization factor of an ellipsoid
m	number of rings
M	A parameter in the coated ellipsoid inclusion model
N	Number of phases in a material
p	Pressure applied to a material (Pa)
$\vec{p}(x)$	Polarization field (W/m ²)
$\langle \vec{p} \rangle$	Volume average polarization field (W/m ²)
$\langle \vec{p} \rangle_i$	Volume average polarization field in inclusion “ i ” (W/m ²)

$\langle \vec{p}_* \rangle_i$	Volume average effective polarization field in the inclusion relative to \underline{k}_* (W/m ²)
\vec{q}	Heat flux vector (W/m ²)
\vec{q}^∞	Heat flux vector at infinity (W/m ²)
$\langle \vec{q} \rangle$	Volume average heat flux vector (W/m ²)
$\langle \vec{q} \rangle_i$	Volume average heat flux vector in a component (W/m ²)
Qr	Power unit length (W/m)
r	Distance from a position vector to the origin of a material (m)
r'	Radius of sensor ring (m)
R _i	Radius of a material (m)
R _n	Electrical resistance of a material at time t (Ω)
R _{no}	Electrical resistance of a material at time 0 (Ω)
T _i	Temperature of a component (K)
$\vec{\nabla} T$	Temperature gradient vector (K)
$\vec{\nabla} T^\infty$	Applied temperature gradient at infinity (K)
$\langle \vec{\nabla} T \rangle$	Volume average temperature gradient (K)
$\langle \vec{\nabla} T \rangle_i$	Volume average temperature gradient vector in a component (K)
t	Time (s)
u	Speed of sound in a material (m/s)
v	Velocity of a material
V _i	Volume of a component
\vec{x}	Position vector
x	Component of the position vector, \vec{x}
y	Component of the position vector, \vec{x}

z	Component of the position vector, \vec{x}
α	Polarizability
α_{in}	In-plane thermal diffusivity in Eq. 4-2 (m ² /s)
$\alpha_{through}$	Through-plane thermal diffusivity in Eq. 4-3 (m ² /s)
β	Principle axes of an ellipsoid
β	Temperature coefficient of resistance (1/K)
δ	Dirac delta function
ε	Standard lack of fit parameter
θ	Parameter determined by volume fraction
λ	Mean free path (m)
ρ	Density of a component (kg/m ³)
σ	Integration variable
τ	Hot Disk equation parameter
ϕ	Volume fraction of a component
ϕ_m	Maximum packing fraction of a component
ψ	Nielsen model equation parameter

Chapter 1: Introduction

1.1: Introduction and Motivation

Most polymer resins are thermally insulating, and increasing the thermal conductivity of these resins allows them to be used in heat sink applications. One emerging market for thermally conductive resins is for bipolar plates in fuel cells. A fuel cell is an electrochemical device that continuously converts chemical energy to electrical energy [1]. There are five main fuel cells (FC): Polymer Electrolyte Membrane (PEMFC), Alkaline (AFC), Phosphoric Acid (PAFC), Molten Carbonate (MCFC), and Solid Oxide (SOFC). PEMFC's have a subset of fuel cells called Direct Methanol (DMFC). There also regenerative fuel cells which are a newer technology being researched by NASA [2]. Each of the main fuel cells are characterized by the type of electrolytes used and the operating temperature range. Table 1.1-1 below [1-5] summarizes the five main fuel cells, and a more extensive summary table of these fuel cells is given in Chapter 2.

The fuel cells summarized have different applications. PEMFC is used for transportation, specialty vehicles, distributed power generation, and portable electrical devices [2, 6]. In a PEMFC hydrogen is used as the fuel. Hydrogen reacts with oxygen (from the air) to produce DC electricity. The byproducts produced from this reaction are heat and water, which makes a PEMFC a better alternative for vehicles [1].

Table 1.1-1: Summary of the Five Main Fuel Cells [1-5]

Fuel Cell	Electrolyte	Operating Temperature (°C)
Polymer Electrolyte Membrane (PEMFC)	Solid organic polymer	30-100
Alkaline (AFC)	Aqueous solution of potassium hydroxide soaked in a matrix	90-100
Phosphoric Acid (PAFC)	Liquid phosphoric acid soaked in a matrix	175-220
Molten Carbonate (MCFC)	Liquid solution of lithium, sodium and/or potassium carbonates, soaked in a matrix	600-700
Solid Oxide (SOFC)	Solid zirconium oxide with a small amount of yttria added	600-1000

Fuel cells are stacked together to reach a desired voltage depending on the application. A bipolar plate separates one cell from the next, and the plate carries hydrogen gas from one side and air (oxygen) to the other side. Bipolar plates require thermal conductivity (to conduct away the heat generated), low gas permeability, and good dimensional stability [1]. Engineering thermoplastics are being researched as an alternative material for bipolar plates in fuel cells. Using thermoplastics is advantageous because it is a light weight material and the material properties can be varied to meet specific requirements [7-9].

This research focuses on the thermal conductivity of the thermoplastic. Typical thermal conductivity values in W/mK for some common materials are given in Table 1.1-2 [10]. One approach to improving the thermal conductivity of a polymer is through the addition of a conductive filler material, such as carbon and metal [11-24]. In a polymer containing conductive fillers heat is transferred by two mechanisms lattice vibrations (major contributor) and electron movement [12]. Generally, a single type of carbon is used in thermosetting resins (often a vinyl ester) to produce a thermally conductive bipolar plate material [25-28]. Thermosetting resins cannot be remelted.

Table 1.1-2: Thermal Conductivity for Common Materials [10]

Materials	Thermal Conductivity (W/m·K)
Polymers	0.2 to 0.30
PAN-based Carbon Fiber	8 to 70
Stainless Steel	11 to 24
Aluminum	218 to 243
Copper	400
Silver	418
Diamond	990

1.2: Objectives

The goal of this M.S. research was to take measured in-plane thermal conductivities and develop models to predict the effective in-plane thermal conductivity for composite materials containing varying amounts of a single filler either carbon black, synthetic graphite, or carbon fiber. In previous research by R.A. Hauser [29] effective in-plane thermal conductivity models have been developed by parameter fitting. In this research the models developed only use physical properties of the composite material constituents, geometry, and information on processing. The composite materials modeled in this research can possibly be used as the material to produce bipolar plates for fuel cells.

1.3: References

1. Thomas, S. and Zalbowitz, M., “Fuel Cells: Green Power”, Los Alamos National Laboratory, LA-UR-99-3231, 1999.
2. “Energy Efficiency and Renewable Energy - Fuel Cells”
http://www1.eere.energy.gov/hydrogenandfuelcells/fuelcells/fc_types.html,
accessed September 2010.
3. Hoogers, G., The Engineering Handbook, 2nd Edition, CRC Press, 2004.
4. Barbely, A.M. and Kreider, J.F., Distributed Generation: The Power Paradigm for the New Millenium, CRC Press, 2001.
5. Larminie, J. and Dicks, A., Fuel Cell Systems Explained, 2nd Edition, John Wiley & Sons Ltd., West Sussex, England, 2003.
6. Baird, D.G., Huang, J., and McGrath, J.E., “Polymer Electrolyte Membrane Fuel Cells: Opportunities for Polymers and Composites”, *Plastics Engineering*, **59** (12), December 2003.
7. Finan, J. M., *Proceedings of the Society of Plastics Engineers Annual Technical Conference*. May 2-6, 1547 (1999).
8. Mapleston, P., “Conductive Composites Get a Growth Boost from Metallic Fibers”, *Modern Plastics*, May 1992, pp. 80-83.

9. Simon, R.M., “Thermally and Electrically Conductive Flake Filled Plastics”, *Polymer News*, Vol. 11, 1985, pp. 102-108.
10. “ADMET Materials Testing Systems – Property Search”,
<http://www.matweb.com/search/SearchProperty>, accessed September, 2010
11. R. Taipalus, T. Harmia, M. Q. Zhang, and K. Friedrich, *Compos. Sci. & Tech.*, **61**, 801 (2001).
12. Y. Agari and T. Uno, *J. Appl. Polym. Sci.*, **30**, 2225 (1985).
13. D. M. Bigg, *Polym. Eng. Sci.*, **17**, 842 (1977).
14. D. M. Bigg, *Adv. Polym. Technol.*, **4**, 255 (1984).
15. M. Narkis, G. Lidor, A. Vaxman, and L. Zuri, *J. Electrostat.*, **47**, 201 (1999).
16. K. Nagata, H. Iwabuki, and H. Nigo, *Compos. Interfaces*, **6(5)**, 483 (1999).
17. A. Demain, “Thermal Conductivity of Polymer-Chopped Carbon Fibre Composites”, Ph.D. Dissertation, Universite Catholique de Louvain, Louvain-la-Neuve, Belgium (1994).
18. J.A. King, K.W. Tucker, J.D. Meyers, E.H. Weber, M.L. Clingerman, and K.R. Ambrosius, *Polym Compos.*, **22** (1), 142 (2001).
19. M. V. Murthy, *Proceedings of the Society of Plastics Engineers Annual Technical Conference*, 1396 (1994).

20. R.M. Simon, Polym. News, 11, 102 (1985).
21. P. Malpeston, Mod. Plast., 69, 80 (1992).
22. J. –B. Donnet, R.C. Bansal, and M. –J. Wang, *Carbon Black*, 2nd edition, Marcel Dekker, Inc, New York (1993).
23. J. –C. Huang, *Adv. Polym. Technol.*, **21**, 299 (2002).
24. D.M. Bigg, Polym. Compos., **8**, 1 (1987).
25. M.S. Wilson and D. N. Busick, U.S. Patent Number 6,248,467: “Composite Bipolar Plate for Electrochemical Cells”, June 19,2001.
26. R. O. Loutfy and M. Hecht, U.S. Patent Number 6,511,766: “Low Cost Molded Plastic Fuel Cell Separator Plate with Conductive Elements”, January 28, 2003.
27. J. C. Braun, J. E. Zabriskie, Jr., J. K. Neutzler, M. Fuchs, and R. C. Gustafson, U. S. Patent Number 6,180,275: “Fuel Cell Collector Plate and Method of Fabrication”, January 30, 2001.
28. V. Mehta and J. S. Cooper, *Journal of Power Sources*, **114**, 32 (2003).
29. R. A. Hauser, J. M. Keith, J. A. King, and J. L. Holdren, *Journal of Applied Polymer Science*, **100**, 2914, (2008).

Chapter 2: Background

2.1: Fuel Cells

Between 1838 and 1839 Friedrich Wilhelm Schobain, a German-Swiss chemist, and William Grove, a physical scientist, discovered the main operating principle of fuel cells. The main operating principle of a fuel cell is the generation of electricity from reversing water electrolysis. A fuel cell is an electrochemical device that continuously converts chemical energy to usable (electrical) energy without combustion. Fuel cells are being developed for the automotive propulsion, electric power generation, and portable systems market [1,2].

Fuel cell technology is an improvement on current battery and engine technology. Fuel cells are similar to batteries and engines. Fuel cells are similar to batteries because they are an electrochemical device that generates power, and fuel cells are similar to engines because they work continuously by consuming fuel [1]. However, fuel cells differ from engines because they operate in a two-step process rather than a four-step process. An engine converts chemical energy to thermal energy, then to mechanical energy, and finally to electrical energy [2]. Fuel cells improve engines because they convert chemical energy directly to electrical energy. Fuel cells are a desirable technology because they are more efficient due to this direct conversion, there are no harmful emissions, and they have low operating noise and temperatures [1, 2].

Fuel cells are comprised of three key components which are the anode, cathode, and electrolyte. To produce electrical energy a fuel is supplied to the anode and an oxidant is supplied to the cathode. The fuel supplied is oxidized by an electrochemical reaction on the surface of the anode and the oxidant is reduced by an electrochemical reaction on the surface of the cathode. These electrochemical reactions create ions which flow through the electrolyte located between the anode and cathode. Electrons are produced on the anode and flow through an external load to the cathode producing electricity. Figure 2.1-1 shows a diagram of a fuel cell [2].

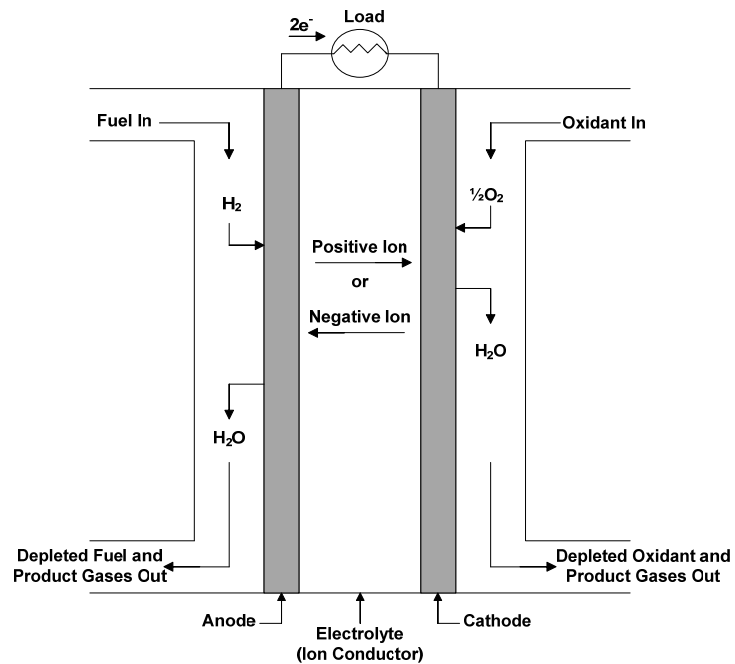
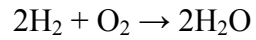


Figure 2.1-1: Diagram of a Fuel Cell [2]

Hydrogen is the desired fuel in a fuel cell due to its high reactivity. Hydrocarbons can also be used as fuel but need to be converted to hydrogen before being used. Oxygen is the desired oxidant because it is readily available in the environment [2]. When hydrogen is the fuel and oxygen is the oxidant the following reaction takes place.



There are five main types of fuel cells and the operating principles are the same for each. The fuel cells differ in the type of electrolyte used, operating temperature, and useful applications. A detailed summary of these fuel cells are shown in Table 2.1-1 below [1-5]. This work involves researching materials that have the potential to be used for a component of the proton exchange membrane fuel cell (PEMFC). More details on the PEMFC will be given in the next section.

Table 2.1-1: Detailed Summary of the Five Main Fuel Cells [1-5]

Fuel Cell Type	Electrolyte	Anode/Cathode Reaction	Operating Temperature	Applications
Proton Exchange Membrane (PEMFC)	Solid organic polymer	$H_2 = 2H^+ + 2e^-$ $\frac{1}{2}O_2 + 2H^+ + 2e^- = H_2O$	30 – 100°C	Transportation, specialty vehicles, portable power and small distributed generation
Alkaline (AFC)	Aqueous solution of potassium hydroxide soaked in a matrix	$H_2 + 2OH^- = 2H_2O + 2e^-$ $\frac{1}{2}O_2 + H_2O + 2e^- = 2OH^-$	90 – 100°C	Used in space and military vehicles
Phosphoric Acid (PAFC)	Liquid phosphoric acid soaked in a matrix	$H_2 = 2H^+ + 2e^-$ $\frac{1}{2}O_2 + 2H^+ + 2e^- = H_2O$	175-220°C	Large number of 200kW combined heat and power systems in use
Molten Carbonate (MCFC)	Liquid solution of lithium, sodium and/or potassium carbonates soaked in a matrix	$H_2 + CO_3^{2-} = H_2O + CO_2 + 2e^-$ $\frac{1}{2}O_2 + CO_2 + 2e^- = CO_3^{2-}$	600-700°C	Suitable for medium-to large-scale combined heat power systems and electrical utility
Solid Oxide (SOFC)	Solid zirconium oxide with a small amount of yttria added	$H_2 + O^{2-} = H_2O + 2e^-$ $\frac{1}{2}O_2 + 2e^- = O^{2-}$	600 – 1000°C	Suitable for all sizes of combined heat and power systems, auxiliary power and electric utility

2.1.1: Proton Exchange Membrane Fuel Cells and Bipolar Plates

The proton exchange membrane fuel cell (PEMFC), also known as the solid polymer fuel cell, is one of the most promising alternative fuel technologies to power cars and buses. PEMFCs have low maintenance because there are no moving parts in the

power generating stacks of the fuel cell system [6]. The electrolyte used in PEMFC is a layer of solid polymer. Hydrogen is the fuel used and it reacts with oxygen (from the air) to produce DC electricity to power motors and auxiliary equipment for the vehicle. The byproduct of this reaction is heat and water [2,7].

Hydrogen gas enters the fuel cell on the anode side, where it encounters a platinum catalyst. The platinum catalyst is used to facilitate the separation of the hydrogen gas into electrons and protons (hydrogen ions). The hydrogen ions pass through the membrane and another platinum catalyst, which helps combine the hydrogen ions, oxygen gas, and electrons on the cathode side to produce water as the product. The electrons that cannot pass through the membrane, flow from the anode to the cathode side of the fuel cell through an external circuit containing a motor or some electric load, which consumes the power generated by the fuel cell. Figure 2.1-2 shows a schematic of a PEMFC with bipolar plates [7].

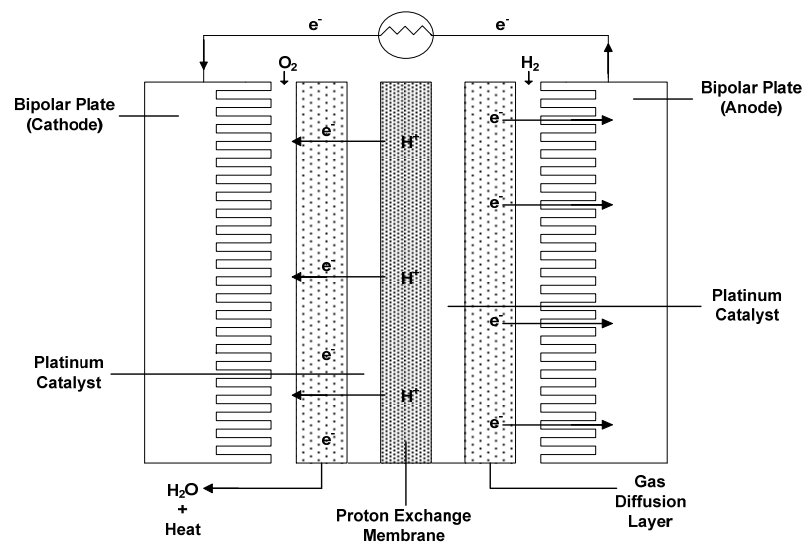


Figure 2.1-2: Schematic of a Proton Exchange Membrane Fuel Cell [8]

The voltage generated from one single fuel cell is approximately 0.7 volts. Since commercial electric motors often operate at 300 volts, fuel cells are stacked in series to produce useful voltage. Key components in a fuel cell stack are current collectors and separator plates. The current collector is used to conduct electrons from the anode to the separator plate, and the separator plate provides the electrical series connection between fuel cells necessary to separate the oxidant flow of one cell from the fuel flow of an adjacent cell. Two current collectors are coupled with a separator plate to form the bipolar plate. There are often 430 bipolar plates needed in a fuel cell stack to achieve 300 volts [2,7].

Bipolar plates are important components of fuel cells and have multiple functions which include connecting individual fuel cells in series, distributing the reactant gases uniformly over the active area, removing excess heat and water, collecting and transporting electrons from the anode to the cathode, and preventing the mixing of the hydrogen and oxygen (reactant gases) [9,10]. To prevent mixing of the reactant gases bipolar plates are made of gas impermeable materials. If the reactant gases mix, then electrons will pass directly from the hydrogen to the oxygen and these electrons cannot be sent to an external circuit to do useful electrical work.

Additionally, bipolar plates must be electrically conductive to minimize ohmic losses and thermally conductive to conduct away generated heat. One anode-cathode cell with an area of 100 cm^2 operating at 1 atm and 80°C (typical PEMFC conditions), producing approximately 0.7V, will generate approximately 1.7 kJ of excess heat and 2.5 kJ of electric energy every minute it operates [6]. Preferably, bipolar plates should be as

thin as possible to minimize electrical resistance and to make the fuel cell stack as small as possible [3,7,11]. Material selection for bipolar plates is based on desired properties, but the plates should also have good dimensional and thermal stability up to 150°C for the next generation of fuel cells [3,12].

2.2: Thermal Conductivity

Thermal conductivity is a unique physical property of materials that describes the rate of heat conduction. Heat is transferred by three mechanisms: conduction, convection, and radiation. In solids, heat transfer is dominated by conduction, and is described by Fourier's Law of Heat Conduction which states that the heat flux is proportional to the temperature gradient. In equation form Fourier's Law is given as [13,14]

$$\vec{q} = -k\vec{\nabla}T, \quad (2-1)$$

where \vec{q} is the heat flux, k is the thermal conductivity, and $\vec{\nabla}T$ is the temperature gradient. The negative sign indicates heat loss so the heat flows from hotter to colder regions, and the thermal conductivity, k , is assumed to be constant for a given material.

Heat can be transferred through solids in many different ways but the most significant mechanisms are electron and phonon transport. In metals, electron transport is the dominant method of heat transfer and in polymers phonon transport is the dominant method [15]. Phonons are the minimal amount of thermal vibrations needed to transmit

energy, and phonons transmit energy through interactions with electrons, protons, neutrons, and other phonons [14]. These interactions can be physically represented as a series of atoms with spring as their bonds. When an atom in series is excited due to heat, pulling or pushing it starts to vibrate. If one atom in the series begins to vibrate then the springs connecting to the other atoms will begin to vibrate, this vibration process will continue with the energy from the original excited atom propagating through the series of atoms. Figure 2.2-1 shows a two-dimensional example of this mechanism [16].

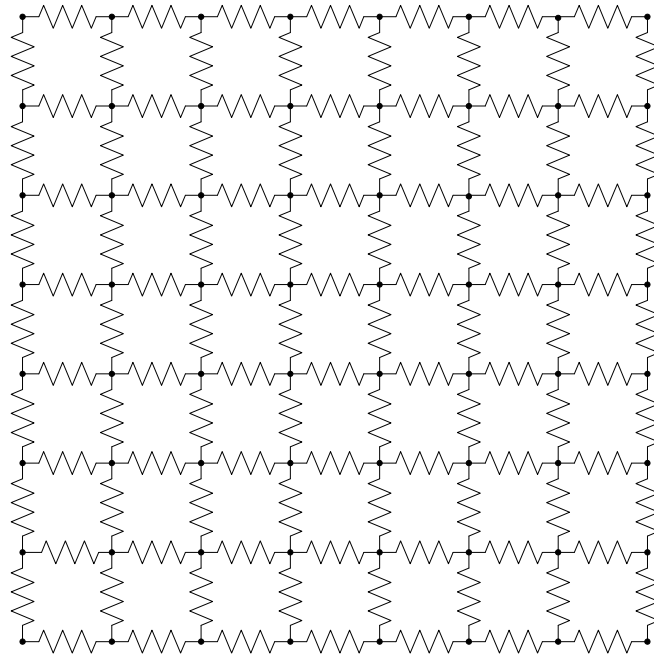


Figure 2.2-1: Two-Dimensional Array of Atoms Connected by Springs [16]

Energy (heat) transfer by phonons is efficient, and the way phonons scatter as they propagate through a material determine the efficiency of this energy transfer [14]. Scattering incidents of phonons occur when a phonon encounters an atom and is either absorbed or deflected into a different direction. A material with a longer distance between

scattering incidents will have a higher thermal conductivity than a material where the distance between scattering incidents is relatively short. This is illustrated in Debye's model for heat conduction in dielectric solids and is given by [15,8]

$$k = \frac{1}{3} \cdot c \cdot u \cdot \lambda . \quad (2-2)$$

In Equation 2-2 k is the thermal conductivity, c is the volumetric heat capacity, u is the velocity of sound in the material, and λ is the mean free path (average distance between scattering incidents) of the phonons in the material. Heat transport by phonons is responsible for transferring thermal energy in polymers composites, and since polymers are dielectric materials they generally follow the Debye model.

2.3: Thermal Conductivity Modeling

Effective properties of polymer composites depend on many factors such as the microstructure of the matrix and filler material, concentration, degree of mixing, orientation, bonding between the filler and matrix, thermal conductivity of the constituents, and the crystallinity of the polymer. It is beneficial to have realistic mathematical models that can accurately predict the effective properties of polymer composites. Understanding the composite thermal behavior under a temperature gradient is important because polymer composite materials have useful applications in the fuel cell industry for bipolar plates. A way to model the thermal behavior of composites is by using math approximations along with the solutions to inclusion problems. In the sections

to follow the solution to the inclusion problem will be given along with approximations used to estimate the effective thermal conductivity of composites.

The effective thermal conductivity of composite can be predicted on a microscopic scale by solving thermal conductivity equations. The thermal conductivity equations are [13,17]

$$\vec{q} = k\vec{\nabla}T \quad (2-3)$$

$$\vec{\nabla} \cdot \vec{q} = 0 \quad (2-4)$$

$$\vec{\nabla} \times \vec{\nabla}T = \vec{0}, \quad (2-5)$$

where \vec{q} is the heat flux vector, k is the thermal conductivity, and $\vec{\nabla}T$ is the temperature gradient vector. Equation 2-3 is the three-dimensional Fourier's Law and Equation 2-4 comes from simplification of the energy equation. The energy equation in terms of temperature change is given as [12]

$$\rho\hat{C}_p \frac{dT}{dt} = -(\vec{\nabla} \cdot \vec{q}) - (\tau : \vec{\nabla}v) - \left(\frac{\partial \ln \rho}{\partial \ln T} \right)_p \frac{dp}{dt}. \quad (2-6)$$

In Equation 2-6, ρ is the density of the composite, \hat{C}_p the heat capacity of the composite, T is the temperature, t is the time, p is the pressure applied to the composite, v is the velocity of the composite, $(\vec{\nabla} \cdot \vec{q})$ is the rate of heat addition by conduction per volume of the composite, $(\tau : \vec{\nabla}v)$ is the rate of heat increase per unit volume by viscous

dissipation, and $\left(\frac{\partial \ln \rho}{\partial \ln T}\right)_p$ is the rate of work done on the composite by external forces.

Equation 2-6 simplifies to Equation 2-4 $(\vec{\nabla} \cdot \vec{q} = 0)$ because $\frac{dT}{dt} = \frac{dp}{dt} = 0$ since the composite is at steady-state meaning there is no change with respect to time, and $(\tau : \vec{\nabla} v) = 0$ because there is no velocity in the solid composite.

On a macroscopic scale the effective thermal conductivity of a composite is determined by measuring the average heat flux and average temperature gradient. The ratio between the average heat flux and average temperature gradient gives the effective thermal conductivity, k_* . So Equation 2-3 can be re-written as

$$\langle \vec{q} \rangle = k_* \langle \vec{\nabla} T \rangle. \quad (2-7)$$

In Equation 2-7 “ $\langle \rangle$ ” denotes volume average in the composite. On the microscopic scale to theoretically compute k_* from Equation 2-7, $\langle \vec{q} \rangle$ and $\langle \vec{\nabla} T \rangle$ must be determined. To determine $\langle \vec{\nabla} T \rangle$ appropriate boundary conditions must be applied and to determine $\langle \vec{q} \rangle$ Equation 2-4 must be satisfied.

When estimating the effective thermal conductivity the rule of mixtures can be used to give an upper bound. The rule of mixtures (also known as the arithmetic mean) is [18]

$$k_* = f_1 k_1 + f_2 k_2, \quad (2-8)$$

where k_* (W/m·K) is the effective thermal conductivity, f_1 is the volume fraction of the filler material, k_1 (W/m·K) is the thermal conductivity of the filler material, f_2 is the volume fraction of the matrix, and k_2 (W/m·K) is the thermal conductivity of the matrix. Likewise to get a lower bound of the effective thermal conductivity the inverse rule of mixtures is used. The inverse rule of mixtures (also known as the harmonic mean) is given as [18]

$$\frac{1}{k_*} = \frac{f_1}{k_1} + \frac{f_2}{k_2} . \quad (2-9)$$

Using these rules of mixtures to set bounds gives a range for the estimated effective thermal conductivity. Equations 2-3 through 2-5 are difficult to solve on a microscopic scale, so as an alternative the solution can be approximated using an inclusion problem with an appropriate approximation method.

2.3.1: Inclusion Problem

An inclusion is a particle with a particular geometry (i.e. spherical, elliptical, etc) that is inserted in a matrix material (in this case, polymer) to form a composite. The matrix material and inclusion have different physical properties and the matrix is assumed to be infinite in all directions. The matrix is subjected to an applied temperature field, and the only inclusion problems with spherical and ellipsoidal geometries can be solved when a field is applied.

Solving the inclusion problem when the inclusion is spherical is complex. For a single sphere with radius, R , and conductivity, k_1 , in an infinite medium with conductivity, k_2 , the temperature gradient can be written using spherical harmonics. The thermal conductivity equations (Eqs. 2-3 through 2-5) are solved for an inclusion with a coated spherical geometry and the solution is given as [19]

$$T(\vec{x}) = \vec{\nabla} T^\infty \cdot \vec{x} - \frac{(k_1 - k_2)}{(k_1 + 2k_2)} (\vec{\nabla} T^\infty \cdot \vec{x}), r \leq R \quad (2-10)$$

$$T(\vec{x}) = \vec{\nabla} T^\infty \cdot \vec{x} - \frac{(k_1 - k_2)}{(k_1 + 2k_2)} \cdot \frac{R^3}{r^3} (\vec{\nabla} T^\infty \cdot \vec{x}), r \geq R \quad (2-11)$$

where T is the temperature, \vec{x} is a position vector from the center of the sphere, k_1 is the thermal conductivity of the spherical inclusion, k_2 is the thermal conductivity of the matrix, R is the radius of the inclusion, r is the distance from the position vector, \vec{x} , to the origin of the inclusion (the magnitude of the vector $r = |\vec{x}|$), and $\vec{\nabla} T^\infty$ is the applied temperature gradient at infinity (applied field) [19].

The inclusion problem can also be solved when the inclusion is an ellipsoid by solving the thermal conductivity equations (Eqs. 2-3 through 2-5). In order to solve this inclusion problem, an ellipsoidal coordinate system is used. Details and results to this inclusion problem can be found in Bohren and Huffman [20], and the solution to this inclusion problem is used in the next section to determine the polarizability of an ellipsoidal inclusion.

There are a variety of different approximations that can be used with the solution to the inclusion problem to estimate the effective thermal conductivity of composites. In the following sections (2.3.3-2.3.6) different approximation methods are discussed.

2.3.2: Polarizability of a Spherical and Elliptical Inclusion

The solution of the inclusion problem can be related to the polarizability of a spherical or elliptical inclusion to estimate the effective thermal conductivity of composites. Approximations used to estimate the effective thermal conductivity of composites make use of the polarizability. To be consistent with the definition of polarizability in linear dielectrics the polarizability, α , of an inclusion is given by [20]

$$\langle \vec{q} \rangle_1 - k_2 \langle \vec{\nabla} T \rangle_1 = \frac{\alpha}{V_1} k_2 \vec{\nabla} T^\infty. \quad (2-12)$$

In Equation 2-12 $\langle \vec{q} \rangle_1$ is the average heat flux in the inclusion, k_2 is the thermal conductivity of the matrix, $\langle \vec{\nabla} T \rangle_1$ is the average temperature gradient in the inclusion, V_1 is the volume of the inclusion, and $\vec{\nabla} T^\infty$ is the external temperature field applied at infinity.

To determine the polarizability, α , the components on the left-hand side of Equation 2-12 are computed by

$$\langle \vec{q} \rangle_1 - k_2 \langle \nabla T \rangle_1 = \frac{1}{V_1} \iiint_{inclusion} (k_1 - k_2) \vec{\nabla} T d\vec{x} . \quad (2-13)$$

In Equation 2-13 the temperature gradient in the inclusion needs to be determined. For the case of a spherical inclusion the temperature gradient in the inclusion is determined from the solution to the inclusion problem in Equation 2-10 which gives

$$\vec{\nabla} T = \vec{\nabla} T^\infty - \frac{(k_1 - k_2)}{(k_1 + 2k_2)} \vec{\nabla} T^\infty , \quad r \leq R \quad (2-14)$$

Substituting Equation 2-14 into Equation 2-13 and performing the triple integration over the volume of the spherical inclusion gives

$$\frac{1}{V_1} \iiint_{inclusion} (k_1 - k_2) \vec{\nabla} T d\vec{x} = (k_1 - k_2) \left[1 - \frac{k_1 - k_2}{k_1 + 2k_2} \right] \vec{\nabla} T^\infty , \quad (2-15)$$

which simplifies to

$$\frac{1}{V_1} \iiint_{inclusion} (k_1 - k_2) \vec{\nabla} T d\vec{x} = \frac{3(k_1 - k_2)k_2}{k_1 + 2k_2} \vec{\nabla} T^\infty . \quad (2-16)$$

Now, Equation 2-16 can be equated to Equation 2-13 giving

$$\langle \vec{q} \rangle_1 - k_2 \langle \vec{\nabla} T \rangle_1 = \frac{1}{V_1} \iiint_{inclusion} (k_1 - k_2) \vec{\nabla} T d\vec{x} = \frac{3(k_1 - k_2)}{k_1 + 2k_2} (k_2 \vec{\nabla} T^\infty) . \quad (2-17)$$

Comparing the right-hand side of Equation 2-17 with the right-hand side of Equation 2-12 shows that the polarizability of the spherical inclusion is [17, 20]

$$\frac{\alpha}{V_1} = \frac{3(k_1 - k_2)}{k_1 + 2k_2} I. \quad (2-18)$$

In Equation 2-18 I is the identity matrix and is needed because the thermal conductivities, k_1 and k_2 , are scalars and the polarizability is a tensor. If the inclusion is an ellipsoid the same outlined steps are followed to determine the polarizability. The polarizability for an ellipsoidal inclusion is given as [17, 20]

$$\frac{\alpha_i}{V_1} = \frac{k_1 - k_2}{k_2 + d_i(k_1 - k_2)} \text{ with } i = 1, 2, 3. \quad (2-19)$$

In Equation 2-19, d_i are the depolarizing factors of the ellipsoid which are defined in more detail in Chapter 5. The depolarizing factors for a sphere are $d_i = 1/3$. The polarizability of an ellipsoid is a tensor with only diagonal entries because the ellipsoidal inclusions in the composite are assumed to be aligned in the horizontal plane of the composite. This means that the semi-axes of the inclusions are aligned with the major axes of the composite. Now the explicit formulas for the polarizability of spherical and ellipsoidal inclusions can be used in approximations for estimating the effective thermal conductivity of composites.

2.3.3: Maxwell-Garnett's Approximation

Maxwell-Garnett's approximation, also known as the Clausius-Mossotti approximation, is a method widely used to estimate effective properties of composite

materials. This approximation is not dependent on the size of the inclusion and can be used to study effective properties of two-component mixtures in which the matrix and inclusion are both isotropic. The particle geometries that can be analyzed using this approximation are spheres and ellipsoids [17].

The Maxwell-Garnett approximation uses the solution to the inclusion problem along with the polarizability to estimate the effective thermal conductivity of a composite. This approximation equates the polarizability of a composite with effective thermal conductivity, k_* , in an infinite matrix of thermal conductivity k_2 . Then the polarizability is set equal to the sum of the polarizabilities of the spherical inclusions of thermal conductivity k_1 in a matrix of thermal conductivity k_2 .

The effective thermal conductivity of a polymer composite consisting of spherical inclusions using Maxwell-Garnett's approximation is given as [21]

$$\frac{k_* - k_2}{k_* + 2k_2} = \frac{f_1 \alpha}{3V_1}, \quad (2-20)$$

where k_* is the effective thermal conductivity, k_2 is the thermal conductivity of the matrix, f_1 is the volume fraction of inclusions, V_1 is the volume of the inclusions, and α is the polarizability in the spherical inclusions. Using the polarizability of a sphere as given in Equation 2-18 gives [17,21,22]

$$\frac{k_* - k_2}{k_* + 2k_2} \approx f_1 \frac{k_1 - k_2}{k_1 + 2k_2} I. \quad (2-21)$$

Solving Equation 2-21 for k_* gives an explicit formula for the effective thermal conductivity of a composite with spherical inclusions. The explicit equation is given as [17,21,22]

$$k_* \approx k_2 \frac{k_1(1+2f_1)+2k_2(1-f_1)}{k_1(1-f_1)+k_2(2+f_1)}. \quad (2-22)$$

Maxwell-Garnett's approximation can also be used to estimate the effective thermal conductivity of a polymer composite with aligned non-spherical inclusions, and the equation is given as [17]

$$k_* \approx k_2 I + f_1 \left(I - \frac{1}{3} f_1 \alpha \right)^{-1} \alpha, \quad (2-23)$$

where α is the polarizability and I is an identity matrix. Equation 2-23 only holds true if the centers of the inclusions are isotropically distributed.

2.3.4: Effective Medium Approximation

The effective medium approximation is another method used to estimate effective properties of polymer composites. This approximation was introduced by Bruggeman and the basis of this approximation is the “self-consistency” assumption. Assume there is a polymer composite made up of two types of spherical inclusions (inclusion 1 and inclusion 2) that fill its entire space. Inclusion 1 has a thermal conductivity k_1 and volume fraction f_1 while inclusion 2 has a thermal conductivity k_2 and a volume fraction f_2 . To

estimate the effective thermal conductivity, k_* , of the composite a small representative sample of the composite is chosen. The sample is chosen in such a way that the inclusions are well-separated from each other which ensures that the proportion of inclusion 1 and inclusion 2 in the sample are equal to the proportion of inclusion 1 and inclusion 2 in the composite [17].

The “self-consistency” assumption states that the effective thermal conductivity of the composite remains equal to k_* when the medium surrounding the representative sample is replaced by a homogeneous effective medium with an effective thermal conductivity of k_* . Combining this assumption with the solution to the inclusion problem for a spherical inclusion in Equation 2-10 gives an equation for the effective thermal conductivity as [17]

$$k_* = \frac{1}{4} \left[\gamma + (\gamma^2 + 8k_1k_2)^{1/2} \right] \quad (2-24)$$

$$\gamma = (3f_1 - 1)k_1 + (3f_2 - 1)k_2. \quad (2-25)$$

The inclusion can also be ellipsoidal in shape. If k_* is isotropic then the results from the ellipsoidal inclusion problem gives an implicit equation for the effective thermal conductivity of the composite [23]

$$\sum_{i=1}^N \sum_{\beta=1}^3 f_i \frac{k_* - k_i^\beta}{(1 - L_i^\beta)k_* + L_i^\beta k_i^\beta} = 0. \quad (2-26)$$

In Equation 2-26 N is the number of phases in the composite, β are the principle axes of the ellipsoid inclusions, k_i^β is the principle conductivities of phase i , and L_i^β is the depolarization factor of the ellipsoidal inclusions. The depolarization factors L_i^β are the same as the depolarization factors d_{ci} and d_{ei} discussed in Chapter 5.

2.3.5: Average Field Approximation

The average field approximation was used by Polder and Van Santen [24] to estimate effective properties of composite materials. The average field approximation uses average fields such as the temperature gradient, heat flux or polarization from the inclusion problem. Like the effective medium approximation this model is based on the “self-consistency” assumption. The general idea of the average field approximation is to write the effective thermal conductivity, k_* , in terms of one the fields and then substitute the corresponding field from the solution to the inclusion problem.

To use the temperature gradient field to estimate the effective thermal conductivity of a composite start with Equation 2-7

$$\langle \vec{q} \rangle = k_* \langle \vec{\nabla} T \rangle. \quad (2-27)$$

The total average temperature gradient in the composite is a weighted average of the temperature gradient in each phase in proportion to its volume fraction so Equation 2-27 can be written as [17]

$$\langle \vec{q} \rangle = k_* \left(f_1 \langle \vec{\nabla} T \rangle_1 + f_2 \langle \vec{\nabla} T \rangle_2 \right). \quad (2-28)$$

Now an expression is needed for the average temperature gradient of each phase in terms of the average heat flux, $\langle \vec{q} \rangle$, in the composite. Consider a composite with spherical inclusions, to get the expression for $\langle \vec{\nabla} T \rangle_1$ and $\langle \vec{\nabla} T \rangle_2$ the solution to the inclusion problem in Equations 2-10 and 2-11 are used.

The same steps can be followed to use the heat flux field to estimate the effective thermal conductivity of a composite. Again starting with Equation 2-7 the average heat flux in the composite can be expressed as a weighted average of the average heat flux in each phase of the composite which gives

$$k_* \langle \vec{\nabla} T \rangle = \left(f_1 \langle \vec{q} \rangle_1 + f_2 \langle \vec{q} \rangle_2 \right). \quad (2-29)$$

In Equation 2-29 $\langle \vec{q} \rangle_1$ is the average heat flux in the inclusion and $\langle \vec{q} \rangle_2$ is the average heat flux in the surrounding medium and they are given by

$$\langle \vec{q} \rangle_1 = k_1 \langle \vec{\nabla} T \rangle_1 \quad (2-30)$$

$$\langle \vec{q} \rangle_2 = k_2 \langle \vec{\nabla} T \rangle_2. \quad (2-31)$$

So Equation 2-29 can be re-written as

$$k_* \langle \vec{\nabla} T \rangle = \left(f_1 k_1 \langle \vec{\nabla} T \rangle_1 + f_2 k_2 \langle \vec{\nabla} T \rangle_2 \right), \quad (2-32)$$

and assuming that the inclusions are spherical $\langle \vec{\nabla} T \rangle_1$ and $\langle \vec{\nabla} T \rangle_2$ can be computed from the solution to the inclusion problem in Equations 2-10 and 2-11.

Lastly the average polarization field, $\vec{p}(x) = \vec{q}(x) - k_2 \vec{\nabla} T(x)$, can also be used to estimate the effective thermal conductivity of a composite. The average polarization field in the composite is a linear combination of the average heat flux and the average temperature gradient field in the composite and is given as

$$\langle \vec{p} \rangle = \langle \vec{q} \rangle - k_2 \langle \vec{\nabla} T \rangle. \quad (2-33)$$

Substituting in Equation 2-7 the average polarization field in the composite is given as

$$\langle \vec{p} \rangle = (k_* - k_2) \langle \vec{\nabla} T \rangle. \quad (2-34)$$

The average polarization in the composite can be expressed as a weighted average of the polarization in each phase of the composite so Equation 2-34 can be expressed as

$$\langle \vec{p} \rangle = f_1 \langle \vec{p} \rangle_1 + f_2 \langle \vec{p} \rangle_2 = (k_* - k_2) \langle \vec{\nabla} T \rangle. \quad (2-35)$$

The polarization field is zero in the matrix material so Equation 2-35 can be simplified to

$$f_1 \langle \vec{p} \rangle_1 = (k_* - k_2) \langle \vec{\nabla} T \rangle. \quad (2-36)$$

Now an expression is needed for the average polarization in the inclusion in terms of the average temperature gradient in the composite. The average polarization in the inclusion is given as

$$\langle \vec{p} \rangle_1 = (k_1 - k_2) \langle \vec{\nabla} T \rangle_1, \quad (2-37)$$

substituting this into Equation 2-36 gives

$$f_1(k_1 - k_2) \langle \vec{\nabla} T \rangle_1 = (k_* - k_2) \langle \vec{\nabla} T \rangle. \quad (2-38)$$

From the inclusion problem, the average temperature gradient in the inclusion is related to the polarizability of the inclusion by

$$\langle \vec{\nabla} T \rangle_1 = (k_1 - k_*)^{-1} \frac{\alpha}{V} k_* \langle \vec{\nabla} T \rangle, \quad (2-39)$$

and when substituted into Equation 2-38 an implicit equation is given for the effective thermal conductivity as

$$f_1(k_1 - k_2) (k_1 - k_*)^{-1} \frac{\alpha}{V} k_* \langle \vec{\nabla} T \rangle = (k_* - k_2) \langle \vec{\nabla} T \rangle. \quad (2-40)$$

When the geometry of the inclusion is a sphere the polarizability in Equation 2-18 can be substituted into Equation 2-40 and an explicit formula for k_* is given as

$$k_* - k_2 = \frac{3f_1(k_1 - k_2)k_*}{k_1 + 2k_2}. \quad (2-41)$$

Equation 2-41 is approximation for the effective thermal conductivity of composite with spherical inclusions. When the inclusion is spherical and isotropic all three average field approximations give the same formula for k_* .

2.3.6: Assemblage of Neutral Inclusions

In a composite a neutral inclusion is an inclusion that does not disturb an applied temperature field. This means that the neutral inclusion can be removed from the composite without changing the properties of the composite while a temperature field is being applied [25]. This section will examine neutral inclusions that have geometries of coated spheres and coated ellipsoids and use an assemblage of each to derive explicit formulas to estimate the effective thermal conductivity of a composite.

An assemblage of coated spheres was introduced by Hashin and Shtrikman in 1962 [17]. The basis of this model is when an appropriate effective thermal conductivity, k_* , is chosen, a sphere of thermal conductivity k_I with coating of the pure matrix at thermal conductivity k_2 can be inserted as an inclusion in an infinite matrix material without disturbing the uniform temperature gradient outside the sphere [17]. Figure 2.3-1 depicts a neutral inclusion.

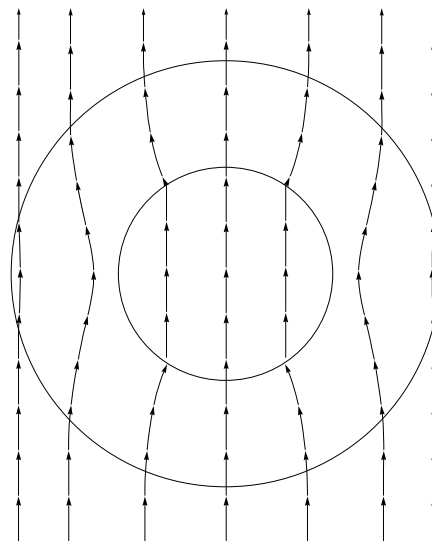


Figure 2.3-1: Neutral Spherical Inclusion

An assemblage of neutral spherical inclusions can have an infinite number of phases. Here a composite with two phases will be considered. The first phase contains an isotropic filler and the second phase contains an isotropic matrix material which acts as a coating on the filler. The first phase is embedded in the second phase. To determine the effective thermal conductivity of the composite the thermal conductivity equations (Eqs. 2-3 through 2-5) must be solved for this inclusion problem. To solve this inclusion problem when a uniform temperature gradient is applied the temperature must be examined in each phase of the inclusion. The temperature is given as [17]

$$T_1(\vec{x}) = \left[a_1 + \frac{b_1}{r^3} \right] z, \text{ in core} \quad (2-42)$$

$$T_2(\vec{x}) = \left[a_2 + \frac{b_2}{r^3} \right] z, \text{ in coating} \quad (2-43)$$

$$T_*(\vec{x}) = \left[a_* + \frac{b_*}{r^3} \right] z, \text{ in effective medium.} \quad (2-44)$$

In Equations 2-42 through 2-44 a_1 is a constant, a_2 is a constant, a_* is constant, b_1 is a constant that equals zero because T_1 is finite, b_2 is a constant, b_* is a constant, \vec{x} is the position vector, $r^2 = x^2 + y^2 + z^2$ which contain the components of vector \vec{x} .

Next the heat flux in each phase is computed using Fourier's Law (Equation 2-3) which gives

$$\vec{q}_1 = \{0, 0, a_1 k_1\}, 0 \leq r \leq R_1 \quad (2-45)$$

$$\vec{q}_2 = \left\{ -\frac{3k_2 b_2 xz}{r^5}, -\frac{3k_2 b_2 yz}{r^5}, k_2 a_2 - \frac{3k_2 b_2 z^2}{r^5} + \frac{k_2 b_2}{r^3} \right\}, R_1 \leq r \leq R_2 \quad (2-46)$$

$$\vec{q}_3 = \left\{ -\frac{3k_*b_*xz}{r^5}, -\frac{3k_*b_*yz}{r^5}, k_*a_* - \frac{3k_*b_*z^2}{r^5} + \frac{k_*b_*}{r^3} \right\}, r \geq R_2. \quad (2-47)$$

Equations 2-45, 2-46, and 2-47 represent the core, coating, and effective medium, respectively, of the spherical neutral inclusion problem and there are five unknowns a_1 , a_2 , a_* , b_2 and b_* . To determine the five unknowns appropriate boundary and jump conditions must be applied and the unknowns are given by the following system of equations

$$a_1 = a_2 + \frac{b_2}{R_1^3} \quad (2-48)$$

$$a_2 + \frac{b_2}{R_2^3} = a_* + \frac{b_*}{R_2^3} \quad (2-49)$$

$$k_1 a_1 = k_2 \left(a_2 - \frac{2b_2}{R_1^3} \right) \quad (2-50)$$

$$k_2 \left(a_2 + \frac{2b_2}{R_2^3} \right) = k_* \left(a_* + \frac{2b_*}{R_2^3} \right) \quad (2-51)$$

$$k_* a_* = 1. \quad (2-52)$$

In Equations 2-48 through 2-52 R_1 is the radius of the core spherical inclusion and R_2 is the radius exterior spherical inclusion. This system of five algebraic equations is solved to determine the constants. Once the constants are known they are substituted back into the heat flux equations (Eqs. 2-45 through 2-47).

Finally to compute the effective thermal conductivity of the composite the average heat flux within the composite must be computed. The average heat flux in the

coated sphere is given by integrating over the volume of the spherical inclusion in polar coordinates

$$\langle \vec{q} \rangle = \langle \vec{q}_1 \rangle + \langle \vec{q}_2 \rangle = \int_0^{R_1} \int \vec{q}_1 dV + \int_{R_1}^{R_2} \int \vec{q}_2 dV = \vec{q}^\infty = \{0, 0, 1\}, \quad (2-53)$$

and solving this equation results in the thermal conductivity, k_* (W/m·K), being given as

$$k_* = k_2 + \frac{3f_1k_2(k_1 - k_2)}{3k_2 + (1 - f_1)(k_1 - k_2)}. \quad (2-54)$$

In Equation 2-54, k_1 (W/m·K) is the thermal conductivity of the filler, k_2 (W/m·K) is the thermal conductivity of the matrix, and f_1 is the filler volume fraction.

Now consider neutral inclusions that are coated ellipsoids. This model is called the assemblage of coated ellipsoids and is an extension of the assemblage of coated spheres model. This model was introduced by G. W. Milton [17], and the basis of this model is the same as the assemblage of coated spheres.

This model can have an infinite number of phases but for simplicity two phases will be considered. The first phase is embedded in the second phase and the first phase is the filler and the second phase is the matrix material which acts as a coating on the filler. In this model the assumption is made that the coated ellipsoids are aligned with the major axis of the composite. This neutral inclusion problem is solved the same as the assemblage of coated spheres using ellipsoidal coordinates. To solve this neutral inclusion problem ellipsoidal coordinates are used and the same steps for solving the assemblage of coated spheres are followed. The details of the solution to this inclusion problem can be found in Milton [17]. Since the ellipsoidal inclusions are assumed to be

aligned the effective thermal conductivity will only have diagonal entries and the effective thermal conductivity, \underline{k}_* (W/m·K), is given by

$$\underline{k}_* = \begin{pmatrix} k_{*[1,1]} & 0 & 0 \\ 0 & k_{*[2,2]} & 0 \\ 0 & 0 & k_{*[3,3]} \end{pmatrix} \quad (2-55)$$

$$k_{*[i,i]} = k_2 + \frac{f_1 k_2 (k_1 - k_2)}{k_2 + (d_{ci} - f_1 d_{ei})(k_1 - k_2)} \quad i = 1, 2, 3. \quad (2-56)$$

In this Equation 2-56, d_{ci} and d_{ei} are the depolarization factors of the core and exterior ellipsoidal inclusions and are a function of the core and exterior semi-axes of the coated ellipsoids. This model is used later in the modeling chapter where more details on the depolarization factors are given (Chapter 5).

2.3.7: Nielsen's Model

This research group has previously done thermal conductivity modeling of composites using a theoretical and curve fitting approach. Composites are generally anisotropic which means that heat conduction in the composite depends on the direction of measurement. Therefore, to determine the effective thermal conductivity of a composite with anisotropic constituents the heat conduction must be measured in the through-plane and in-plane direction. Similarly one way to model the effective thermal conductivities of a composite is to develop two separate models; through-plane and in-plane [16].

One model this research group has used is Nielsen's model. Nielsen model predicts the through-plane thermal conductivity of a composite. This model is based on a model developed by Albert Einstein for the viscosity of a fluid with dispersed spheres [26,27] and the Halpin-Tsai equations for calculating the elastic moduli of composites [26]. Einstein's model and the Halpin-Tsai model were not developed to predict the thermal conductivity of composites but can be extended to predict the through-plane thermal conductivity of two phase composites.

Nielsen's model made modifications to the Halpin-Tsai model by changing nomenclature and incorporating a new term ψ which accounts for the orientation and packing of the filler in the matrix. The Halpin-Tsai equations, only took into account the shape of the filler. Nielsen's model is given as [26,28]

$$k_{through} = k_2 \left(\frac{1 + AB\phi}{1 - B\psi\phi} \right) \quad (2-57)$$

$$B = \frac{\left(\frac{k_1}{k_2} - 1 \right)}{\left(\frac{k_1}{k_2} + A \right)} \quad (2-58)$$

$$\psi \cong 1 + \frac{1 - \phi_m}{\phi_m^2} \phi. \quad (2-59)$$

In Equations 2-57 through 2-59, $k_{through}$ is the through-plane thermal conductivity of the composite, k_1 and k_2 are the thermal conductivities of the filler and the polymer, respectively, ϕ is the volume fraction of the filler, A is a shape and orientation factor, and

B is a factor that takes into account the relative conductivity of the two components. Finally, the ψ parameter relates the maximum packing fraction ϕ_m to the filler and polymer volume fractions. The parameter A can theoretically be calculated by [26,28]

$$A = 1 - k_e, \quad (2-60)$$

where k_e is the Einstein coefficient. Some values for A have already been determined for specific filler types and are given Table 2.3-1 [13]. The maximum packing fraction ϕ_m has also been determined for specific filler shapes and orientations and are given in Table 2.3-2 [13].

Table 2.3-1: Shape Factor ‘A’ for Common Filler Types [13]

Filler Type	Aspect Ratio	A
Cubes	1	2
Spheres	1	1.5
Random Fibers	2	1.58
Random Fibers	4	2.08
Random Fibers	6	2.80
Random Fibers	10	4.93
Random Fibers	15	8.38
Uniaxially Oriented Fibers	--	$2L/D^{(a)}$
Uniaxially Oriented Fibers	--	$0.5^{(b)}$

^a Heat flow in direction of fibers

^b Heat flow transverse to fiber direction

Table 2.3-2: Maximum Packing Fraction of Selected Fillers [13]

Particle Shape	Packing order	ϕ_m
Spheres	Hexagonal Close	0.7405
Spheres	Face Centered Cubic	0.7405
Spheres	Body Centered Cubic	0.60
Spheres	Simple Cubic	0.524
Spheres	Random Loose	0.601
Spheres	Random Close	0.637
Irregular	Random Close	~ 0.637
Fibers	Three Dimensional Random	0.52
Fibers	Uniaxial Hexagonal Close	0.907
Fibers	Uniaxial Simple Cubic	0.785
Fibers	Uniaxial Random	0.82

To show how well Nielsen's model predicted the through-plane thermal conductivity experimental data, a standardized lack of fit term, ϵ was calculated using. A value of $\epsilon = 0$ would indicate a perfect fit of the experimental data with the model. Nielsen's model was shown to underestimate and overestimate the experimental data so the shape factor A and packing fraction ϕ_m were adjusted to give a $\epsilon \approx 0$ [16]. The results from this modeling work are in Hauser's Dissertation [16].

There is not a lot of experimental data for the in-plane thermal conductivity of composites and as a result there are not many models that predict the in-plane thermal conductivity of composites. However, research has been conducted by Keith et al. and Miller et al. and they have developed an empirical model to predict the in-plane thermal conductivity of carbon-filled liquid crystal polymer composites [29,30]. The in-plane model showed that the square root of the product of the through-plane and in-plane

thermal conductivities is an exponential function of the filler volume fraction, ϕ , which is [27,28]

$$\sqrt{k_{in}k_{through}} = Ce^{D\phi}. \quad (2-61)$$

In Equation 2-61, k_{in} is the in-plane (longitudinal) thermal conductivity, $k_{through}$ is the through-plane (transverse) thermal conductivity, ϕ is the volume fraction filler, and C and D are parameters obtained through fitting an exponential trend to the experimental data.

In conclusion, the models discussed in sections 2.3.3-2.3.6 use a “first-principles” modeling approach to estimate the effective thermal conductivity of composites. Using first-principles the effective thermal conductivity of the composite is estimated based on information about the physical properties of the constituents that make up the composite. While past thermal conductivity modeling done by this research group, used a mixed approach of both first-principles and empirical modeling to estimate the through- and in-plane thermal conductivity of a composite. The advantage to using a “first-principles” modeling approach is that experimental work can be reduced.

2.4: References

1. Hoogers, G., The Engineering Handbook, 2nd Edition, CRC Press, 2004.
2. Barbely, A.M. and Kreider, J.F., Distributed Generation: The Power Paradigm for the New Millenium, CRC Press, 2001.
3. Larminie, J. and Dicks, A., Fuel Cell Systems Explained, 2nd Edition, John Wiley & Sons Ltd., West Sussex, England, 2003.
4. Thomas, S. and Zalbowitz, M., “Fuel Cells: Green Power”, Los Alamos National Laboratory, LA-UR-99-3231, 1999.
5. “Energy Efficiency and Renewable Energy - Fuel Cells”,
http://www1.eere.energy.gov/hydrogenandfuelcells/fuelcells/fc_types.html,
accessed September 2010.
6. Thomas, S. and Zalbowitz, M., “Fuel Cells: Green Power”, Los Alamos National Laboratory, LA-UR-99-3231, 1999.
7. Gottesfeld, S., Keller, C.F., Moller-Holst, S., Redondo, A., and Milliken, J., “Fuel Cells: Green Power”, Los Alamos National Laboratory, LA-UR-99-3231, 1999.
8. Hauser, R. A., “Synergistic Effects and Modeling of Thermally Conductive Resins for Fuel Cell Bipolar Plate Applications”, Ph.D. Dissertation, Michigan Technological University, Houghton, MI, 2008.

9. Hermann, A., Chaudhuri, T., and Spagnol, P., “Bipolar Plates for PEM Fuel Cells: A Review”, *International Journal of Hydrogen Energy*, **30**, 1297-1302, 2005.
10. Baird, D.G., Huang, J., and McGrath, J.E., “Polymer Electrolyte Membrane Fuel Cells: Opportunities for Polymers and Composites”, *Plastics Engineering*, **59** (12), December 2003.
11. “Fuel Cells”, Los Alamos National Laboratory, <http://www.lanl.gov/orgs/ee/fuelcells/index.shtml>, 2002, accessed September 2010.
12. United States Department of Energy, Multi-Year Research, Development, and Demonstration
http://www1.eere.energy.gov/hydrogenandfuelcells/mypp/pdfs/fuel_cells.pdf, accessed September 2010.
13. Bird, R.B., Stewart, W.E., and Lightfoot, E.N., Transport Phenomena, 2nd Edition, Wiley, New York, NY, 2002.
14. Bigg, D.M., “Thermally Conductive Polymer Compositions”, *Polymer Composites*, **7** (3), 125, 1986.
15. Berman, R., Thermal Conduction in Solids, Clarendon Press, Oxford, NY, 1976.
16. Weber, E.H., “Development and Modeling of Thermally Conductive Polymer/Carbon Composites”, Ph.D. Dissertation, Michigan Technological University, Houghton, MI, 2001.

17. G. W. Milton, The Theory of Composites, Cambridge University Press, New York, 2002.
18. Foster, D. M. E. and Phillips, G. M., “The Arithmetic-Harmonic Mean”, *Mathematics of Computations*, **42**, 183-191, 1984.
19. Torquato, S., *Random Heterogeneous Materials: Microstructure and Macroscopic Properties*, Springer, New York, 2001.
20. Bohren, C. F. and Huffman, D. R., Absorption and Scattering of Light by Small Particles, Wiley, New York, 1983.
21. Ruppin, R., “Evaluation of extended Maxwell-Garnett theories”, *Optic Communication*, **182**, 273-279, 2000.
22. Gao, L., “Maxwell-Garnett type approximation for nonlinear composites with shape distribution”, *Physical Letters A*, **309**, 435-442, 2003.
23. Noh, T. W., Song, P.H., and Sievers, A. J., “Self-consistency conditions for the effective medium approximation in composite materials”, *Physical Review B*, **44** (11), 5459-5464, 1991.
24. Polder, D. and Van Santen, J., “The Effective Permeability of Mixtures of Solids”, *Physica XII*, **5**, 257-271, 1946.
25. Milton, G. W. and Serkov, S. K., “Neutral coated inclusions in conductivity and anti-plane elasticity”, *Mathematical, Physical and Engineering Sciences*, **457** (2012), 1973-1997, 2001.

26. Nielsen, L.E., “The Thermal and Electrical Conductivity of Two-Phase Systems”, *I & EC Fundamentals*, **13** (1), 17-20, 1974.
27. Nielsen, L.E. and Landel, R.F., Mechanical Properties of Polymers and Composites, 2nd Edition, Marcel Dekker, New York, NY, 1994.
28. Progelhof, R.C., Throne, J.L., and Ruetsch, R.R., “Methods of Predicting Thermal Conductivity of Composite Systems: A Review”, *Polymer Engineering and Science*, **16** (9), 221-257, 1975.
29. Keith, J.M., King, J.A., Miller, M.G., and Tomson, A.M., “Thermal Conductivity of Carbon Fiber/Liquid Crystal Polymer Composites”, *Journal of Applied Polymer Science*, **102**, 5456-5462, 2006.
30. Miller, M.G., Keith, J.M., King, J.A., Edwards, B.J., Klinkenberg, N., and Schiraldi, D.A., “Measuring Thermal Conductivities of Anisotropic Synthetic Graphite-Liquid Crystal Polymer Composites”, *Polymer Composites*, **27** (4), 388-394, 2006.

Chapter 3: Materials

3.1: Materials

The materials used in this research were a polymer matrix and three carbon fillers. The polymer matrix used was Ticona's Vectra A950RX liquid crystal polymer that has advantageous properties for fuel cell bipolar plates. The three carbon fillers used were Akzo Nobel's Ketjenblack EC-600 JD carbon black, Asbury Carbons' Thermocarb TC-300 synthetic graphite, and Toho Tenax America's Fortafil 243 carbon fiber. More details on these materials is given in the following sections.

3.2: Matrix Material

3.2.1: Vectra A950RX Liquid Crystal Polymer

The matrix material used in this research was Ticona's Vectra A950RX liquid crystal polymer (LCP). Vectra is a highly ordered thermoplastic copolymer consisting of 73 mol % hydroxybenzoic acid (HBA) and 27 mol % hydroxynaphthoic acid (HNA). This LCP has the properties needed for bipolar plates, namely high dimensional stability up to a temperature of 250°C, short molding times (often 5-10 s), exceptional dimensional reproducibility, chemical resistance in acidic environments present in fuel cells, and a low hydrogen gas permeation rate [1, 2]. The chemical structure and physical properties of this polymer are shown in Figure 3.2-1 [3] and Table 3.2-1 [1], respectively.

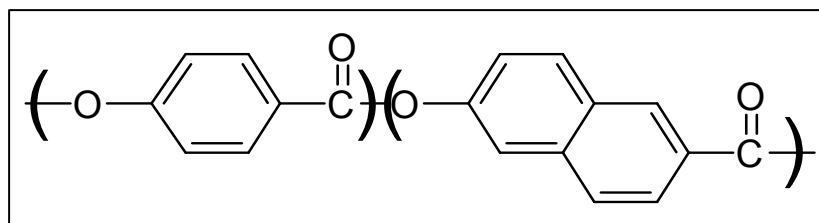


Figure 3.2-1: Chemical Structure for Vectra A950RX LCP [3]

Table 3.2-1: Properties of Ticona's Vectra A950RX LCP [1]

Melting Point	280 °C
Tensile Modulus (1mm/min)	10.6 GPa
Tensile Stress at break (5mm/min)	182 MPa
Tensile Strain at break (5mm/min)	3.4%
Flexural Modulus at 23 °C	9.1 GPa
Notched Izod Impact Strength at 23 °C	95 kJ/m ²
Density at 23 °C	1.40 g/cc
Volumetric Electrical Resistivity at 23 °C	10 ¹⁵ ohm-cm
Surface Electrical Resistivity	10 ¹⁴ ohm
Thermal Conductivity at 23 °C	0.22 W/m·K (approx.)
Humidity Absorption (23 °C/50% RH)	0.03 wt%
Mold Shrinkage-parallel	0.0%
Mold Shrinkage-normal	0.7%
Coefficient. of linear thermal expansion- parallel	0.04 x 10 ⁻⁴ /°C
Coefficient. of linear thermal expansion- normal	0.38 x 10 ⁻⁴ /°C

3.3: Filler Materials

3.3.1: Carbon Black

Carbon black is one of the top 50 industrial chemicals manufactured worldwide, and currently 18 billion pounds of carbon black are produced per year. Carbon black is a black fine pellet or powder and is produced by two different manufacturing processes. The first and most common method is furnace black processing. In furnace black

processing a heavy aromatic oil is used as the feedstock. The oil feedstock is reduced to separate atoms in a closed reactor under controlled conditions. The feedstock then enters a hot gas stream where it is vaporized and pyrolyzed to form microscopic carbon particles [4].

The thermal black process is another method used to produce carbon black. In this process natural gas containing methane or heavy aromatic oil is used as the feedstock material. The natural gas is injected into a hot refractory lined furnace with no air and the heat from the refractory material decomposes the natural gas to carbon black and hydrogen. The carbon black produced may be further processed to remove impurities [4].

Common uses for carbon black are reinforcing and conductive agent in high performance materials such as tires, plastics, electrostatic discharge compounds, toners and printing inks. Carbon black is also used for pigmentation and ultraviolet stabilization [4]. As a reinforcing agent carbon black can be added to materials to improve physical properties such as tensile strength and wear resistance. As a conducting agent carbon black can increase the electrical and thermal conductivity of a material.

For this research Akzo Nobel supplied Ketjenblack EC-600 JD. This is an electrically conductive carbon black filler and the physical properties are given in Table 3.3-1 [5] below. Carbon black is sold in the form of pellets that are 100 μm to 2 mm in size. When mixed with a polymer, the pellets easily separate into primary agglomerates 30-100 nm long. Carbon black is highly branched and has a high surface area allowing it to contact a large amount of polymer which results in improved electrical conductivity at low carbon black concentrations [5]. Figure 3.3-1 shows carbon black [3].

Table 3.3-1: Properties of Akzo Nobel Ketjenblack EC-600 JD [5]

Electrical Conductivity	10-100 S/cm
Aggregate Size	30-100 nm
Specific Gravity	1.8 g/cm ³
Apparent Bulk Density	100-120 kg/m ³
Ash Content, max	0.1 wt%
Moisture, max.	0.5 wt%
BET Surface Area	1250 m ² /g
Pore Volume	480-510 cm ³ /100g



Figure 3.3-1: Carbon Black [3]

3.3.2: Synthetic Graphite

Synthetic graphite is manufactured by high temperature treatment of amorphous carbon materials. The main feedstocks used to produce synthetic graphite are calcined petroleum coke and coal tar pitch. One method to produce synthetic graphite is to take a carbonaceous gas such as acetylene, subject it to prolysis, and precipitate the graphite carbons formed [6]. Synthetic graphite is sometimes used as an anode in aqueous electrolytic processes. Other uses for synthetic graphite are in batteries, pencils, polymer composites, and fuel cells, crucibles, refractory products, and lubricants [7-9].

The synthetic graphite used in this work is Asbury Carbons' Thermocarb TC-300 synthetic graphite, previously sold by Conoco [10, 11]. Table 3.3-2 shows the properties of this synthetic graphite. Thermocarb TC-300 is produced from a thermally-treated, highly aromatic petroleum feedstock and contains very few impurities. The average particle size of the synthetic graphite is approximately 70 μm and the aspect ratio is approximately 1.7 [10]. Figure 3.3-2 shows an ESEM photomicrograph of this synthetic graphite [3].

Table 3.3-2: Properties of Thermocarb TC-300 Synthetic Graphite [10]

Carbon Content, wt%	99.91
Ash, wt%	< 0.1
Sulfur, wt%	0.004
Density, g/cm ³	2.24
BET Surface Area, m ² /g	1.4
Thermal Conductivity at 23°C, W/mK	600 in "a" crystallographic direction
Electrical Conductivity of bulk carbon powder at 150 psi, 23°C, parallel to pressing axis, S/cm	50
Particle Shape	Acicular
Particle Aspect Ratio	1.7
Sieve Analysis	wt %
+600 microns	0.19
+ 500 microns	0.36
+300 microns	5.24
+ 212 microns	12.04
+180 microns	8.25
+150 microns	12.44
+75 microns	34.89
+44 microns	16.17
-44 microns	10.42

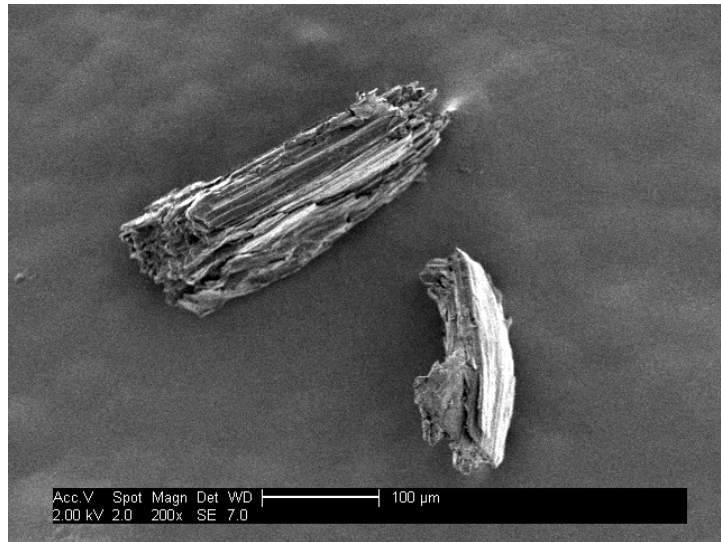


Figure 3.3-2: Thermocarb TC-300 Synthetic Graphite ESEM Image at 200X Magnification [3]

3.3.3: PAN-Based Carbon Fiber

Carbon fiber is a high-performance material that has been commercially available for over 50 years. Carbon fiber is a fibrous material with 90% carbon content, and is produced from organic precursors and by gas growth. Cotton, linen, polyamide, and polyvinyl chloride are some naturally occurring materials that have been previously used to produce carbon fiber [12]. Currently, carbon fiber is manufactured from rayon, acrylic, mesophase pitch, cellulosic, and polyacrylonitrile (PAN) precursors [12, 13]. PAN is the most common precursor used today. More details on the production of PAN-based carbon fiber are given below.

Approximately 70% to 80% of carbon fiber produced is PAN-based. Figure 3.3-3 below shows the chemical structure of PAN-based carbon fiber. It is advantageous to produce carbon fiber from the PAN precursor because the chemical structure allows for

faster pyrolysis, it decomposes before melting, it has a higher degree of preferred orientation, and it has a high carbon yield of about 50% to 55% when pyrolyzed to 1000°C or higher [12].

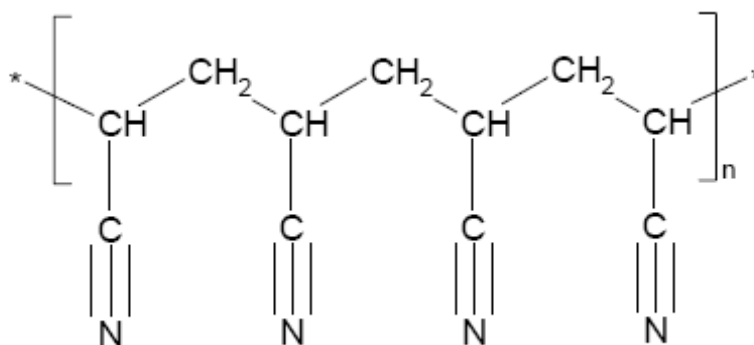


Figure 3.3-3: Structural Formula of Polyacrylonitrile (PAN) [12]

Figure 3.3-4 below gives the process flow diagram for the main steps used to produce PAN-based carbon fiber. The first step is polymerization. In this step the acrylic precursor is produced by polymerizing acrylonitrile and a comonomer by either solution polymerization or solvent-water suspension polymerization. Some comonomers used to produce the acrylic precursor are acrylic acid, methacrylic acid, methacrylate, acrylamide, and itaconic acid. The second step is spinning, and in this step the PAN fibers are formed [12].

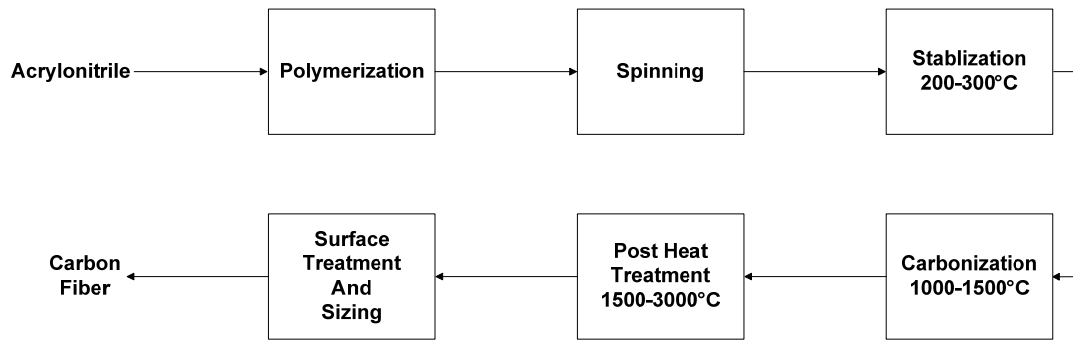


Figure 3.3-4: Process Steps of Carbon Fiber Production from Polyacrylonitrile [12]

Stabilization is the third step in the process for PAN-based carbon fiber production. In this step, the PAN fibers are heated under tension at low temperatures ranging from 200°C to 300°C in an oxidative atmosphere. During this step the chemical structure of the PAN fibers become thermally stable to any additional high temperature heat-treatments. Three reactions take place during stabilization and they are cyclization, dehydrogenation, and oxidation. The PAN fibers also change from their original yellow color to black which is the final color of the carbon fibers. This step is very important because it governs the final structure and mechanical properties of the carbon fiber. The fourth step in carbon fiber production is carbonization. In this step the PAN fibers are converted to carbon fibers. During carbonization the PAN fibers are heated at high temperatures ranging from 1000°C to 1500°C under low tension, and all elements are removed except carbon [12].

After carbonization, the carbon fiber goes through a post heat treatment step; the fifth step in carbon fiber production. In the post heat treatment step the carbon fibers are heated under tension in an inert atmosphere to temperatures ranging from 1500°C to 3000°C. During this step the carbon fibers are increased in size and the crystallites are

aligned, which improves the final properties of the fiber. The final step of the carbon fiber production process is surface treatment. The final carbon fibers produced are surface treated to increase adhesion [12].

Toho Tenax America, Inc.'s supplied Fortafil 243 PAN carbon fiber for this research. This carbon fiber was chosen because of its ability to improve the electrical conductivity, thermal conductivity, and tensile/flexural strength of the Vectra A950RX liquid crystal polymer matrix. Fortafil 243 was surface treated and formed into pellets by the manufacturer. A proprietary polymer (sizing) was used as a binder for the pellets to promote adhesion with the matrix. Table 3.3-3 lists the properties of the carbon fiber [14] and Figure 3.3-5 and Figure 3.3-6 show ESEM micrographs images of this filler [3].

Table 3.3-3: Properties of Toho Tenax America's Fortafil 243 Carbon Fiber [14]

Tensile Strength	3800 MPa
Tensile Modulus	227 GPa
Electrical Resistivity	16.7 $\mu\text{ohm-m}$
Thermal Conductivity	20 W/m K (axial direction)
Bulk Density	356 g/liter
Fiber Diameter	7.3 μm
Filament Shape	Round
Fiber Mean Length	3.2 mm (entire range is 2.3 mm to 4.1 mm)
Carbon Assay	95%
Binder Content	2.6 wt% proprietary polymer that adheres pellet together and promotes adhesion with nylon

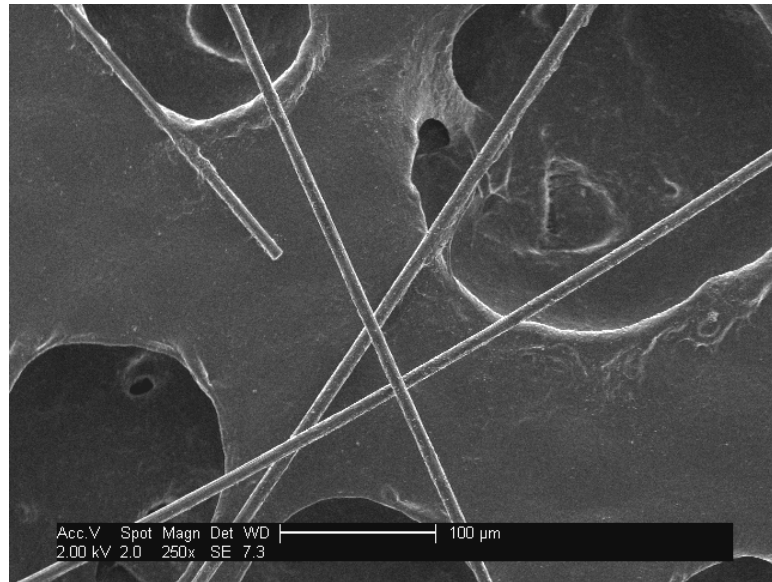


Figure 3.3-5: Fortafil 243 Carbon Fiber ESEM Image at 250X Magnification [3]

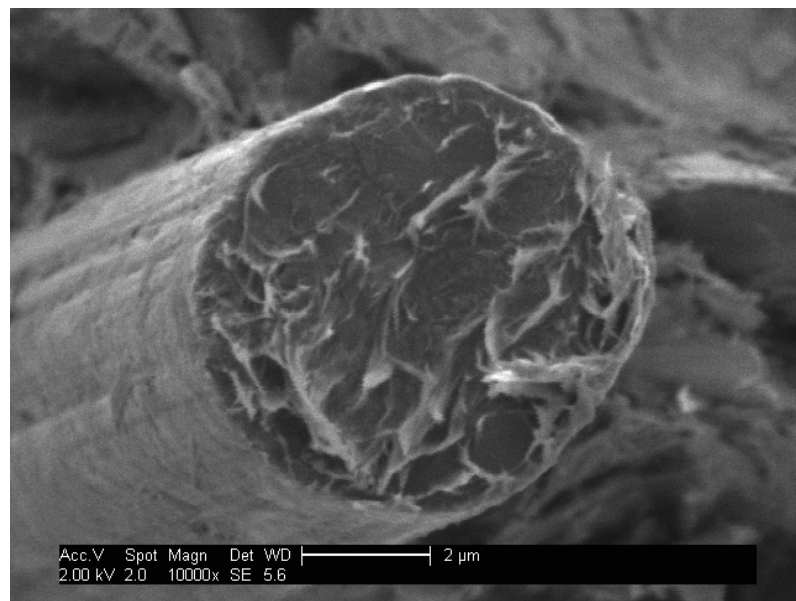


Figure 3.3-6: Fortafil 243 Carbon Fiber ESEM Image at 10000X Magnification [3]

3.3.4: Formulation Naming Convention

For this project, it was important to name and number each specimen. Each test specimen produced was labeled according to the filler type and weight percent. The filler types were abbreviated as follows “CB” is carbon black (Ketjenblack EC-600JD), “SG” is synthetic graphite (Thermocarb TC-300), and “CF” is carbon fiber (Fortafil 243). The concentrations for all the single filler composites tested in this research are shown in Table 3.3-4.

Table 3.3-4: Single Filler Loading Levels

Formulation	Filler wt%	Filler vol%
Vectra	0	0
2.5CB	2.5	1.9
4CB	4.0	3.1
5CB	5.0	3.9
6CB	6.0	4.7
7.5CB	7.5	6.0
10CB	10.0	8.0
15CB	15.0	12.1
10SG	10.0	6.5
15SG	15.0	9.9
20SG	20.0	13.5
25SG	25.0	17.2
30SG	30.0	21.1
35SG	35.0	25.2
40SG	40.0	29.3
5CF	5.0	4.1
7.5CF	7.5	6.1
10CF	10.0	8.2
15CF	15.0	12.4
20CF	20.0	16.8
25CF	25.0	21.2
30CF	30.0	25.5
35CF	35.0	30.2
40CF	40.0	34.9
45CF	45.0	39.7
50CF	50.0	44.6
55CF	55.0	49.6
60CF	60.0	54.7

3.4: References

1. Ticona Vectra Liquid Crystal Polymer (LCP) Product Information, Ticona, Summit, NJ, 07901, 2000.
2. Chiou, J. S. and Paul, D. R., *J. Polym. Sci. Part B: Polymer Physics*, **25**, 1699, 1987.
3. Hauser, R. A., “Synergistic Effects and Modeling of Thermally Conductive Resins for Fuel Cell Bipolar Plate Applications”, Ph.D. Dissertation, Michigan Technological University, Houghton, MI, 2008.
4. “International Carbon Black Association – What is Carbon Black”, http://www.carbon-black.org/what_is.html, accessed September 2010.
5. Akzo Nobel Electrically Conductive Ketjenblack Product Literature, 300. S. Riverside Plaza, Chicago, IL, 60606 (1999).
6. “Ashbury Carbons – Graphite”, <http://www.asbury.com/Graphite.html#synthetic>, accessed September 2010.
7. Mantell, C.L., Carbon and Graphite Handbook, John Wiley & Sons, Inc., New York, NY, 1968.
8. <http://www.cgm-inc.net> – Accessed September 25, 2010.
9. <http://www.azom.com/details.asp?ArticleID=1630> – Accessed September 25, 2010.
10. Asbury Carbons Product Information, Asbury, NJ, 08802, 2004
11. Conoco Carbons Products Literature, Conoco, Inc., P.O. Box 2197, Houston, TX, 77252-2197 (1999).

12. Donnet, J.B., Wang, T.K., Peng, J.C.M., and Rebouilland, Carbon Fibers, 3rd Edition, Marcel Dekker, Inc., New York, NY, 1998.
13. Peebles, L.H., Carbon Fibers: Formation, Structure, and Properties, CRC Press, Inc., Boca Raton, FL, 1995.
14. Toho Tenax America, Inc. Fortafil Carbon Fibers Technical Data Sheet, 121 Cardiff Valley Road, Rockwood, TN 37854.

Chapter 4: Fabrication and Experimental Methods

4.1: Fabrication Methods

The details of the test specimen preparation will be discussed in this section. All the experimental work for this project was previously done by Dr. Julie King's research group, including Rodwick Barton and Rebecca Hauser. The experimental methods are shown here to aide the reader, and this project focuses on thermal conductivity modeling.

4.1.1: Drying

The polymer matrix material used for this project, Vectra A950RX LCP, was received as pellets and dried. Vectra was dried for 24 hours in an indirectly heated dehumidifying drying oven manufactured by Bry Air Systems. Vectra was dried at 150°C in 20 pound batches and once all of the polymer pellets were dry they were stored in moisture barrier bags. A picture of the Bry Air Dryer is shown in Figure 4.1-1. The carbon fillers were not dried; they were used as received.



Figure 4.1-1: Bry Air Dryer System

4.1.2: Extrusion

An extruder was used to produce the polymer composite material researched in this project. An American Leistritz Corporation Model ZSE 27 extruder was used. This extruder has a length/diameter ratio of 40, a 27 mm co-rotating intermeshing twin screw design, and 10 independent heating zones. This screw design is used to achieve large concentrations of carbon fillers in the polymer composite to give maximum thermal conductivity. A picture of this extruder is given in Figure 4.1-2 below, and the screw design used can be found in Appendix A.

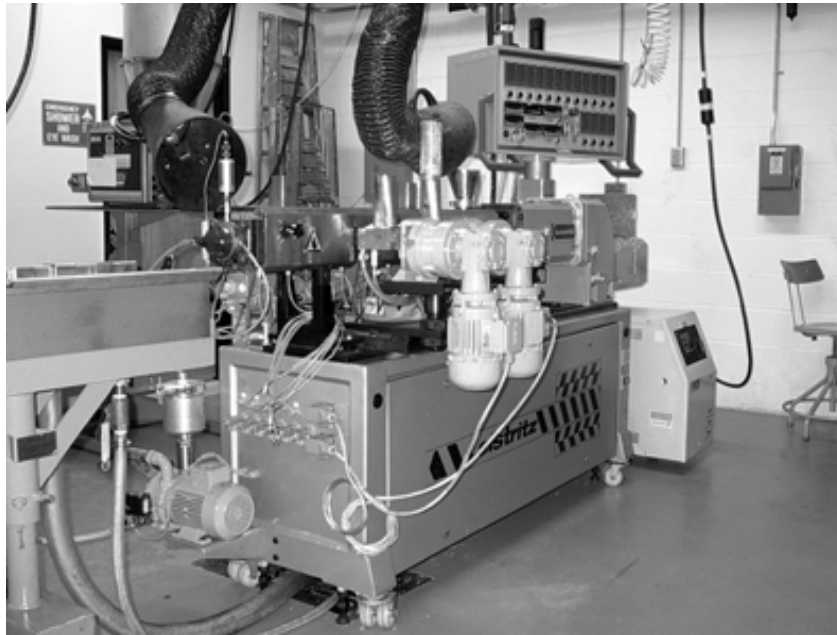


Figure 4.1-2: American Leistritz Extruder with 27 mm Twin Screw

Again, the extruder used in this project had 10 zones. The Vectra polymer pellets were added to Zone 1 of the extruder using a Schenck AccuRate Flexwall gravimetric feeder. Zone 1 was cooled with water to prevent the polymer from obstructing the feed port. A picture of the Schenck AccuRate Flexwall gravimetric feeder is shown in Figure

4.1-3. To produce a polymer composite containing a single carbon filler, the carbon filler was added to Zone 5 of the extruder. The carbon filler was added using a side stuffer fed by AccuRate Conisteel loss in weight feeder which is shown in Figure 4.1-4. Zones 4 and 9 were vented to the atmosphere. Zones 2, 3, 6, 8, and 10 were closed during extrusion. Three extruded strands (3 mm diameter) were produced using this extrusion process.



Figure 4.1-3: AccuRate Flexwall Feeder



Figure 4.1-4: AccuRate Conisteel Feeder

Next, the polymer composite strands entered a water bath for cooling. After cooling, a ConAir Model 204HP-14A pelletizer was used to make 3 mm long pellets from the polymer composite strands. The polymer composite pellets were dried and placed in moisture barrier bags. A picture of the pelletizer and water bath is shown in Figure 4.1-5 below. The specific conditions used in this extrusions process can be found in Appendix B of Hauser's dissertation [1].



Figure 4.1-5: Water Bath & Pelletizer

4.1.3: Injection Molding

After extruding the polymer composite a NE85UA₄ Niigata injection molding machine was used to fabricate the test specimens [2]. This Niigata injection molding machine has a length/diameter ratio of 18, a 40 mm diameter single screw design, a maximum clamp force of 82.5 U.S. tons, a maximum injection pressure of 22, 610 psig,

and a maximum screw speed of 320 rpm. A picture of this injection molding machine is shown in Figure 4.1-6.



Figure 4.1-6: Niigata Model NE85UA₄ Injection Molding Machine

A four-cavity mold, Figure 4.1-7, was used to produce 3.2 mm thick and 6.4 cm diameter disks (end gated) [3]. The specific injection molding conditions for each composite formulation are shown in Appendix C of Hauser's dissertation [1]. The following paragraphs outline the procedure used to injection mold the polymer composite samples.

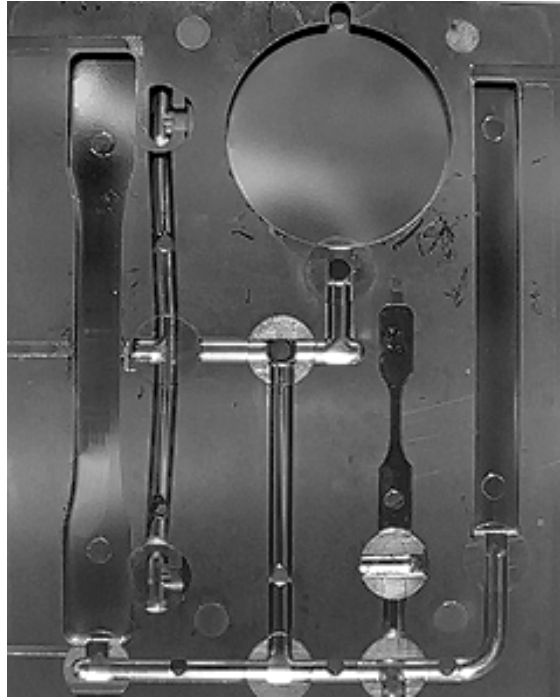


Figure 4.1-7: Four-Cavity Mold

The injection molding machine was turned on and set to the operating temperature of the material being molded. After the operating temperature was reached, the injection molding machine was purged of any contaminants using pure Vectra. About 2lbs of each polymer composite material formulation was molded into 30 disks with 6.4 cm diameter. The injection pressure and the shot size typically were the only adjusted parameters within each formulation. These parameters were adjusted to completely fill the mold. The test specimens formed were stored in low-density polyethylene (LDPE) bags.

After 30 disks were made from one formulation, the injection molding machine was run until it was empty. Next, another formulation was added to the hopper and injection molded. The first 5 disks molded were thrown out because they could still have some of the previous formulation present. During this molding of the first 5 disks the injection

molding machine was optimized for the new material. Next, the 30 disks for the new material were made using the steps outlined above. Finally, at the end of each day, the injection molding machine was cleaned by running pure Vectra through the system. Pure Vectra was molded until the disks contained minimal or no carbon. And lastly, polypropylene was run through the injection molding machine to purge the Vectra and any remaining carbon from the system.

4.2: Experimental Test Methods

Prior to conducting thermal conductivity testing, all samples were conditioned at 23°C and 50% relative humidity for 88 hours in accordance with ISO 291 [4], which is the standard test protocol for Vectra A950RX LCP.

4.2.1: Hot Disk Specific Heat

A Heat Capacity Cell manufactured by Hot Disk Incorporated was used to measure the specific heat of the fabricated polymer composite materials. The 6.4 cm disk produced from injection molding was obtained and three 25 mm diameter and 3.2 mm thick disks were cut from the center. The 25 mm diameter disks were stacked in an insulated copper cup which had a sensor with nickel attached to the bottom. Using a constant power supply, the sensor measured temperature change by detecting the change in resistivity of the nickel. The temperature change in the empty copper cup was compared to the temperature change of the copper cup containing the polymer composite. The specific heat of the polymer composite was determined from these measured

temperature changes. Results from this test are located in Appendix E of Hauser's dissertation [1].

4.2.2: Hot Disk Thermal Analyzer for Transverse and Longitudinal Thermal Conductivity

A Hot Disk Thermal Constants Analyser, manufactured by Hot Disk Incorporated was used in this research. The Hot Disk Thermal Constant Analyser is a technology used to measure longitudinal (in-plane) and transverse (through-plane) thermal conductivity of anisotropic materials. The Hot Disk Thermal Constant Analyser uses transient plane source technique and the thermal conductivities were measured at 23 °C. Figure 4.2-1 below shows a picture of the analyser.



Figure 4.2-1: Hot Disk Thermal Constants Analyser

This test system contained sensors which consisted of a 10 μm thick nickel foil positioned between two 25.4 μm thick layers of Kapton polyimide film. Figure 4.2-2 shows a diagram of the sensors. The polymer composite samples tested had a thickness of 3.2 mm and a diameter of 6.4 cm. To make certain that the heat from the test system was not completely going through the samples in the through-plane direction the assumption of an infinite sample had to be satisfied. To accomplish this, two sample disks were stacked above and below the sensor for a total of four sample disks tested in one run. Stacking the disks allowed for an infinite sample to be tested and the thermal conductivity data collected was reproducible. For each formulation, five sets of disks were (so a total of 20 disks) tested.

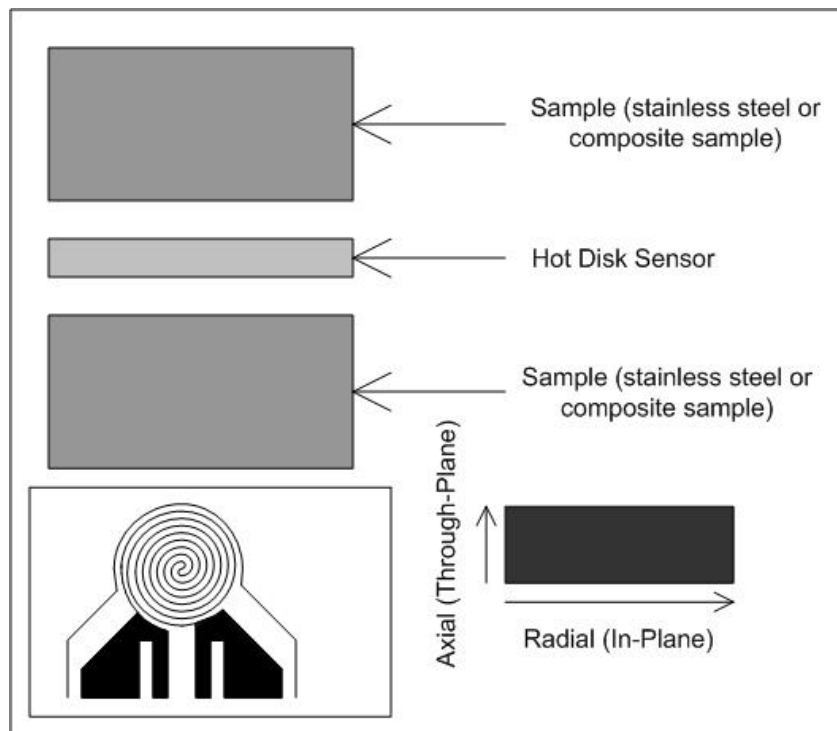


Figure 4.2-2: Diagram of Samples and Sensor. The insert at the lower left shows the double spiral heating element.

A constant power is supplied to the sensor for short periods of time for each test sample. The power supplied and time period varied depending on the sample being tested in the range of 0.03W – 1.25W and 2.5s – 40s, respectively. During testing, heat was generated in the test sample and was dissipated using a double spiral and then conducted through the Kapton insulating layer to the surrounding test samples. This caused a rise in temperature for the sensor and the test sample.

Theoretically, the double spiral can be estimated as a series of concentric equally spaced ring sources. Assuming radial symmetry the heat conduction equation for the double spiral is given as,

$$(\rho C_p) \frac{\partial T}{\partial t} = k_{in} \frac{1}{r} \left(\frac{\partial}{\partial r} \left(r \frac{\partial T}{\partial r} \right) \right) + k_{through} \frac{\partial^2 T}{\partial z^2} + \sum_{rings} Q_r \delta(r - r') \delta(z). \quad (4-1)$$

In Equation 4-1 ρ is the density of the sample (kg/m^3), C_p is the heat capacity of the sample ($\text{J/kg}\cdot\text{K}$), T is the temperature of the sample (K), t is the measurement time (s), k_{in} is the in-plane thermal conductivity of the sample ($\text{W/m}\cdot\text{K}$), r is the radius of the sample, $k_{through}$ is the through-plane thermal conductivity of the sample ($\text{W/m}\cdot\text{K}$), δ is the Dirac delta function, r' is the radius of one of the ring sources, and Q_r is the power supplied to that ring per unit length of the ring (W/m). The total power for each ring is proportional to the circumference of the ring $2\pi r'$, such that the total power supplied for all of the rings is Q (W). This total power Q is an input parameter to the Hot Disk Thermal Constants Analyser. The first term in Equation 4-1 represents accumulation of thermal energy, the second term radial (referred to as in-plane in our experiments) heat conduction, the third term axial (often referred to as through-plane) heat conduction, and the final term is a heat source.

If the experimental time is much less than the characteristic thermal diffusion time, then the sample can be approximated as an infinite domain. For an anisotropic material with a cylindrical geometry, the experimental time must meet the following two criteria [5-9],

$$t \ll (D/2)^2 / (\alpha_{in}) \quad (4-2)$$

$$t \ll T^2 / (\alpha_{through}). \quad (4-3)$$

In Equations 4-2 and 4-3 α is the thermal diffusivity and is given as $\alpha = k / (\rho C_p)$, which is the thermal diffusivity of the polymer composite material.

The average transient temperature increase of the sensor is simultaneously measured by recording the change in electrical resistance of the nickel sensor [5-9] according to,

$$\Delta T = \frac{1}{\beta} \left(\frac{R_n}{R_{no}} - 1 \right), \quad (4-4)$$

where ΔT (K) is the change in temperature at time t , β is the temperature coefficient of resistance of the material (1/K), R_n is the electrical resistance of the nickel at time t (Ω), and R_{no} is the electrical resistance of the nickel at time 0 (Ω). In Equation 4-4 the temperature rise is correlated with the in-plane and through-plane thermal conductivities through the solution to Equation 4-1 as,

$$\Delta T = \frac{P}{\pi^{3/2} R \sqrt{k_{in} k_{through}}} F(\tau), \quad (4-5)$$

$$\tau = \sqrt{\alpha_{thru} t / R^2}. \quad (4-6)$$

In Equation 4-5, $F(\tau)$ is a dimensionless time dependent function of τ and is given by an integral of a double series over the number of rings m

$$F(\tau) = [m(m+1)]^{-2} \int_0^\tau \sigma^{-2} \left[\sum_{l=1}^m l \sum_{k=1}^m k \exp\left(-\frac{l^2 + k^2}{4m^2 \sigma^2}\right) I_0\left(\frac{lk}{2m^2 \sigma^2}\right) \right] d\sigma. \quad (4-7)$$

A detailed derivation of Equations 4-5 and 4-7 is given by He [10].

The complete results for the through-plane and in-plane thermal conductivity of each test specimen can be found in Appendix F in Hauser's dissertation [1]. For this project, the through-plane and in-plane thermal conductivity was measured only for the neat Vectra samples. For all other formulations, only the in-plane thermal conductivity is reported.

4.2.3: Density

The density of the sample disks were measured using the standard test method for density and specific gravity of plastics by displacement, ASTM D792-98 [11]. The sample disk was weighed while dry and then weighed when placed in water. The temperature of the water was noted, and the actual density of the sample was determined using the following equation,

$$\rho_{actual} = \frac{DryWeight}{DryWeight - WetWeight} \cdot \rho_{Water}(T). \quad (4-8)$$

The theoretical density of the sample disk was determined by,

$$\rho_{theoretical} = \frac{1}{\sum_i \frac{\phi_i}{\rho_i}}. \quad (4-9)$$

In Equation 4-9, ρ_i is the density of the constituents of the sample disk, ϕ_i is the volume fraction of the constituents, and i is the type of constituent in the sample disk. The results for each sample can be found in Appendix G in Hauser's dissertation [1]. In all cases, the actual and theoretical composite densities were similar.

4.2.4: Solvent Digestion

Solvent digestion was used to dissolve the polymer composite samples, and ASTM D5226-98, a standard practice for dissolving polymer materials, test method was used [12]. The purpose of this test is to liberate the carbon fiber and synthetic graphite fillers from the polymer matrix. Once this was accomplished the aspect ratio and length of the carbon fiber and synthetic graphite were measured, and these measurement techniques are outlined in the next section. Carbon black was too small (primary aggregate 30-100nm) to be separated using this test method.

A 0.2 g sample was obtained from the center of the 6.4 cm diameter sample disk, and a total of three solvent digestion samples were obtained from each formulation. The 0.2 g sample was placed in a 2 ounce labeled glass vial filled approximately halfway, enough to dissolve the sample, with diethylenetriamine (DETA). A recording of the exact amount of DETA was not necessary because DETA was pulled through the filler and disposed of following regulations. The sample was soaked in DETA for about four to six hours at 170 °F until the polymer matrix was completely dissolved.

While the sample was dissolving, filter paper and a Petri dish were weighed separately using a four-place Denver Instruments A-250 scale, and the weights were recorded. The filter paper used was produced by Millipore and called Duapore ®

membrane filters. These filter papers had a pore size of 0.45 μm . The Petri dish was labeled to make sure the correct filter was used for the correct sample. One filter paper was used for each sample.

After the polymer matrix was dissolved, the polymer/filler/solvent solution was filtered. The filtering system used is shown below in Figure 4.2-3. The filtering system contained a Fisher Brand 47 mm microanalysis filter assembly, vacuum flask, and vacuum pump. The weighed filter paper was placed in the filtration system and the polymer solution was introduced into the filter. The vacuum pulled the solvent and polymer matrix through the filter paper and only the filler material remained on the filter paper. The 2 ounce sample vial was rinsed with isopropyl alcohol to ensure that all of the polymer/filler/solvent solution has been filtered. The funnel was also rinsed with isopropyl alcohol to ensure only filler remained on the filter paper. The vacuum continued to run until all liquid was removed. The filter paper containing the filler was placed in a pre-weighed labeled Petri dish. The Petri dish was placed in the fume hood and left open over night for the filler to dry. These steps were repeated for three samples of each formulation of the polymer composite.

The polymer composite containing carbon black was not dissolved and filtered because the carbon black would plug the filter. After drying the sample overnight the Petri dish with the filter paper and filler was weighed. The weight percent of the filler was determined using the following equation,

$$Wt\% = \frac{Wt_{Final} - Wt_{Filter(s)} - Wt_{PetriDish}}{Wt_{Composite}} \quad (4-10)$$

The complete set of results can be found in Appendix H in Hauser's dissertation [1].

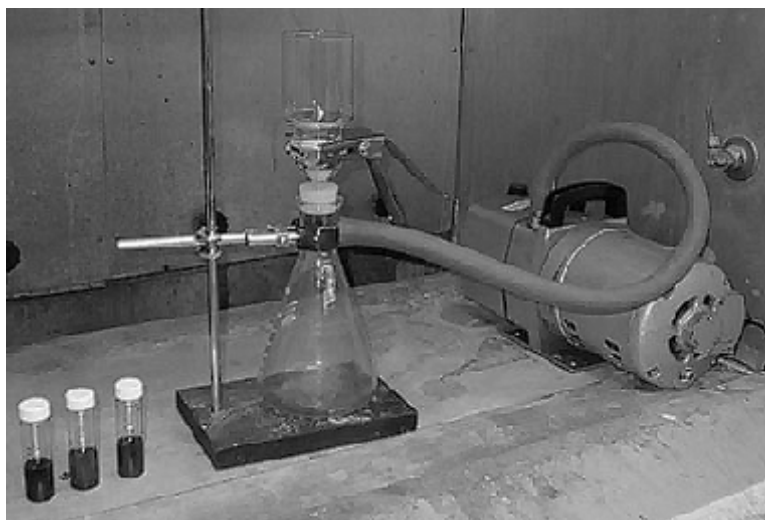


Figure 4.2-3: Solvent Digestion Filtration Apparatus

4.2.5: Filler Length and Aspect Ratio

The carbon fiber and synthetic graphite fillers liberated by solvent digestion were used to determine the aspect ratio and length of the fillers. The “as-received” carbon fiber and synthetic graphite were also measured to determine the aspect ratio and filler length. The two measured values were compared to see if the material changed during extrusion and injection molding.

The fillers were dispersed on a glass slide and the apparatus used to do so is shown in Figure 4.2-4. Approximately 0.01 g of the filler was obtained from the filter paper using a micro-spatula and with the one-hole stopper removed the filler was placed in the crucible. The filler particles were distributed on the glass slide so that no particles were overlapping in the images. The one-hole stopper was replaced in the flask and the flask was placed over the clean surface of the glass slide. A duster can was placed

through the one-hole stopper and the filler was dispersed onto the glass slide using a short burst. After each dispersion, the apparatus and the glass slide were cleaned.

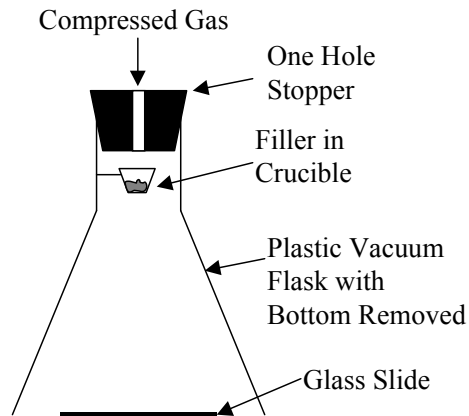


Figure 4.2-4: Filler Dispersion Apparatus

The glass slide containing the dispersed filler was placed on a Prior automatic stage for microscope setup. An Olympus SZH10 optical microscope was used for imaging the dispersed fillers. This microscope contained an Optronics Engineering LX-740 video camera for digital imaging. A picture of the microscope and camera is shown in Figure 4.2-5. An automated series of steps in Scion Image version 1.62 was used to collect the images. Dr. Larry Sutter, professor and director of Michigan Tech's Transportation Institute, wrote the automated steps and they were modified for this project. All of the images were collected at 70x magnification and the results are in Appendix I of Hauser's dissertation [1].

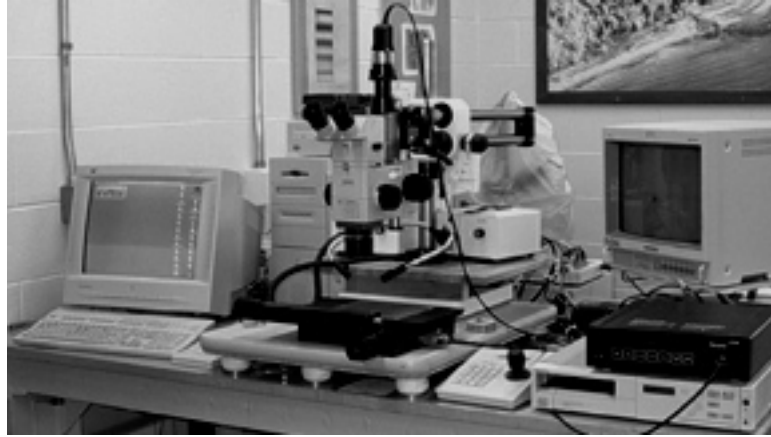


Figure 4.2-5: Microscope Setup Used for Filler Length and Aspect Ratio

The images collected were measured and processed an academic version of Adobe Photoshop 5.0 along with a The Image Processing Tool Kit version 3.0. Batch operation was used for processing of the images, using the following steps [13]:

1. Convert image from red/green/blue (RGB) to grayscale
2. Remove the uneven lighting of the image by fitting and removing the background
3. Standardize the contrast of the image by automatic leveling
4. Convert the image to a binary image where all fillers are in black using threshold
5. Remove all features that came in contact with the edge of the image using feature cutoff and threshold
6. Calibrate image, a predetermined calibration based on the magnification and resolution of the image is loaded
7. Measure all, 26 different items of each feature in the image were measured and stored to a text file that was appended to for each new image

500 to 5000 particles were measured for each formulation. An algorithm was used to measure the maximum and minimum caliper distance of each feature. Every 11.25° the caliper length and height were measured for every feature, and from this a length (maximum caliper distance) and breadth (minimum caliper distance) were calculated. The aspect ratio of the filler is calculated by dividing length by breadth. This method did not work well for particles that were long and thin. This issue was addressed by dividing the length of the fibers by literature diameter to produce the aspect ratio.

4.2.6: Determination of Particle Orientation in the Composite

The method described below was primarily developed by Rodwick Barton Carter with the advice of Buehler and Dr. Karl Peterson, research assistant professor and director of Michigan Tech's Material Characterization Program.

4.2.6.1: Sample Preparation

A 13 mm by 13 mm square was cut out of the center of each of the 3.2 mm thick thermal conductivity samples to generate the in-plane (x-y plane) samples studied. An epoxy mixture was poured into the sample holders and the composite samples were carefully pushed down into the epoxy. A two-part epoxy called Epoxide Cold Mounting Resin and Hardener purchased from Mager Scientific was used. The epoxy was mixed by weight in a ratio of five parts resin to one part hardener. The epoxy plugs cured overnight at room temperature. After curing the epoxy plugs were removed from the sample holders.

4.2.6.2: Polishing

After the epoxy samples cured and were removed from the holder the resulting pucks were polished. The pucks were polished so that images could be taken of the surface using an optical microscopy. First, a 60 grit 12''' abrasive pad was used to ground the epoxy pucks on two sides to shape them as an oval. Next, the epoxy pucks were labeled and attached to the glass microscope slide using JB Kwik Weld. Figure 4.2-6 shows the ground epoxy pucks.

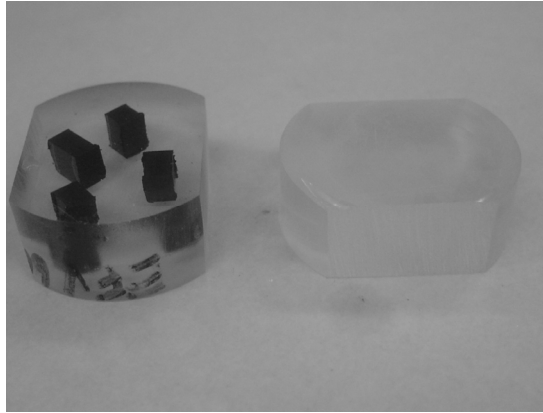


Figure 4.2-6: Ground Oval-Shape Epoxy Pucks

Once the weld was dry and the pucks were secured to the microscope slides the epoxy covering the sample surface is removed. The epoxy is removed using a diamond surface grinder with a vacuum holder. After the epoxy is removed the samples are washed with water and detergent and dried. Another microscope slide with one side frosted is obtained and attached to the puck with the frosted side down using Epotech 301 epoxy. Figure 4.2-7 below shows the prepared puck.

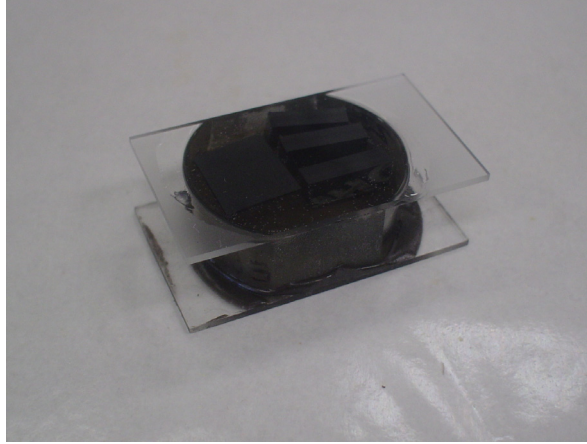


Figure 4.2-7: Prepared Polymer Puck

Next, using a diamond tipped pen the puck samples are labeled on the frosted side of the glass slide. The sample pucks are placed with the frosted side down on a vacuum chuck. A vacuum is applied to hold the sample pucks in place. A cut off saw is used to cut a thin 0.2 mm section from the sample pucks. The thin puck samples are placed in a diamond surface grinder which made the surface of the pucks flat. Figure 4.2-8 shows a picture of the cut off saw and Figure 4.2-9 shows the flat thin puck samples.



Figure 4.2-8: Image of Cut Off Saw Used to Cut Epoxy Puck into Thin Sections

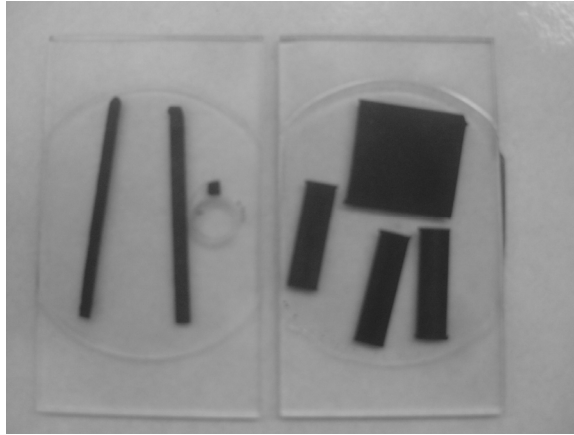


Figure 4.2-9: Thin Sections of Composite Samples Ready for Polishing

The Buehler Ecomet 4 Grinder/Polisher is used to polish the flat thin puck samples, and Figure 4.2-10 shows a picture of the polisher. First, the scratches created from the diamond surface grinding of the sample pucks were removed by using the Buehler Ultra-Pol PSA 12" diameter cloth with Buehler 9 μm Metadi Supreme Polycrystalline Diamond suspension at 120 rpm for 2 minutes.



Figure 4.2-10: Buehler Ecomet 4 Grinder/Polisher

After the diamond scratches were removed the Texmet 1000 polishing cloth (PSA 12" diameter) was used with the 3 μm Metadi Supreme Polycrystalline Diamond suspension at 120 rpm for 4 minutes. The sample pucks were viewed under the microscope to be sure the fillers were clearly visible. If the fillers were not visible then the sample puck was polished again with the 3 μm diamond suspension for 4 minutes. The last step is to use polish the sample pucks with the Master-Tex polishing cloth (PSA 12" diameter) with the Masterprep 0.05 μm polishing suspension at 120 rpm for 2 minutes. The sample puck was viewed with the microscope to be sure that the fillers could be seen which meant that polishing was complete. If the fillers were not able to be seen then the last polishing step was repeated.

4.2.6.3: Optical Imaging Methods

The Olympus BX60 microscope was used to image the polished samples. The magnification used on this microscope was 100x and 200x. Images of the sample pucks were taken across the thickness of the sample using the Scion Image versions 1.62. The images were taken in the direction of the thermal conductivity test. The images collected were put together to get a large composite image for analysis. Appendix J in Hauser's dissertation [1] shows the resulting photomicrographs. Figure 4.2-11 shows a picture of the Olympus BX60.



Figure 4.2-11: Olympus BX60 Microscope

4.3: References

1. Hauser, R. A., “Synergistic Effects and Modeling of Thermally Conductive Resins for Fuel Cell Bipolar Plate Applications”, Ph.D. Dissertation, Michigan Technological University, Houghton, MI, 2008.
2. Niigata Engineering CO. Ltd., Nagaoka Works, Model NE85UA4, Machine No. 50031F. Nagaoka Works, Niigata, Japan.
3. Four Cavity Mold, Master Precision Molds, Inc., Greenville, MI, Phone No. 800-632-8912.
4. International Organization for Standardization (ISO). Plastics – Standard Atmospheres for Conditioning and Testing; ISO 291; 1997, 1998.
5. Gustavsson, M.; Karawacki, E.; Gustafsson, S. E. Rev. Sci. Instrum., **65** (12), 3856-3859, 1994.
6. Log, T., Gustafsson, S. E. Fire and Materials, **19**, 43-49, 1995.
7. Bohac, V., Gustavsson, M. K., Kubicar, L., Gustafsson, S. E. Rev. Sci. Instrum., **71**(6), 2452-2455, 2000.
8. Hot Disk Thermal Constants Analyser Instruction Manual, Mathis Instruments, Ltd., Fredericton, New Brunswick, Canada, 2001.
9. Transient Plane Source – Gustafsson Hot Disk Technique, Standards for Contact Transient-Measurements of Thermal Properties, National Physical Laboratory, United Kingdom, accessed October 2007 at <http://www.npl.co.uk/thermal/ctm/>.
10. He, Y., Thermochemica Acta, **436**, 122-129, 2005.

11. “Specific Gravity and Density of Plastics by Displacement”, ASTM Standard D792 - 66 (Re-approved 1975), American Society for Testing and Materials, Philadelphia, Pennsylvania, 1986.
12. “Standard Practice for Dissolving Polymer Materials”, ASTM Standard D5226 - 98, American Society for Testing and Materials, Philadelphia, Pennsylvania, 1998.
13. Weber, E.H., “Development and Modeling of Thermally Conductive Polymer/Carbon Composites”, PhD Dissertation, Michigan Technological University, 2001.

Chapter 5: In-Plane Thermal Conductivity Modeling

5.1: In-Plane Thermal Conductivity Modeling

The in-plane thermal conductivity of polymer composites depend on many factors such as the microstructure of the matrix and filler material, concentration, degree of mixing, orientation, bonding between the filler and matrix, thermal conductivity of the constituents, and the crystallinity of the polymer. A way to model the thermal behavior of composites is by using math approximations along with the solutions to inclusion problems.

5.2: Modeling Theory

Mathematical models are used in this project to estimate the effective in-plane thermal conductivity. The effective thermal conductivity is computed using Fourier's Law, which states that "the heat flux by conduction is proportional to the temperature gradient" [1]. In equation form Fourier's Law [1] is given as

$$\langle \vec{q} \rangle = \underline{k_*} \langle \vec{\nabla} T \rangle, \quad (5-1)$$

where $\langle \vec{q} \rangle$ is the volume average heat flux vector, $\underline{k_*}$ is the effective thermal conductivity tensor, and $\langle \vec{\nabla} T \rangle$ is the volume average temperature gradient vector.

To determine $\underline{k_*}$, $\langle \vec{q} \rangle$ and $\langle \vec{\nabla} T \rangle$ need to be estimated and one way to accomplish this is by solving an inclusion problem. The "assemblage of ellipsoidal inclusions" is the

general model used for this research. Variations of this model were used for carbon/Vectra A950RX composites. In the ellipsoid inclusion problem, particles inside the polymer composite are assumed to have an ellipsoid shape within a homogenous medium. The ellipsoidal particle is inserted as an inclusion within an infinite homogeneous medium, in which a uniform temperature gradient is applied. Two variations of the assemblage of ellipsoid inclusion model were used; they were the “uncoated ellipsoid assemblage” and the “coated ellipsoid assemblage.” In the modeling developments that follow “ $\underline{\quad}$ ” is used to denote tensors and “ $\vec{\quad}$ ” is used to denote vectors.

5.2.1: Synthetic Graphite and Carbon Black Models

Polder and Van Santen [2] were the first to use uncoated ellipsoids and the average field approximation to estimate effective properties of materials. Others that have worked on solving this inclusion problem are Milton, Helsing, Kirkpatrick, Noh, and Stroud [3-7]. In the average field approximation there are a variety of average fields that can be used from the inclusion problem, and they are the temperature gradient, heat flux, or polarization (a linear combination of both the temperature gradient and the heat flux).

The average polarization, $\langle \vec{p} \rangle$, is defined as

$$\langle \vec{p} \rangle = \langle \vec{q} \rangle - \underline{k}_m \vec{\nabla} T, \quad (5-2)$$

where $\langle \vec{q} \rangle$ is the average heat flux, \underline{k}_m is the thermal conductivity of the matrix, and $\langle \vec{\nabla} T \rangle$ is the average temperature gradient. Polarization is zero in the matrix material and therefore using polarization is advantageous because the average field only needs to

be computed in the ellipsoid particle, not in the surrounding effective medium. Thus, the polarization average field approximation with uncoated ellipsoid inclusions is used to predict in-plane thermal conductivities of the synthetic graphite/Vectra A950RX and carbon black/Vectra A950RX polymer composites.

The effective in-plane thermal conductivity of synthetic graphite/Vectra A950RX and carbon black/Vectra A950RX is determined by the thermal conductivities of the filler and matrix, the volume fraction of the filler, and the polarizability of the inclusion. An explicit formula for predicting the effective thermal conductivity, \underline{k}_* (W/m·K), was derived from concepts in Milton [3] and extending the results of Helsing and Helte [4]. The derivation is summarized below in the following sections.

Starting with the definition of the average polarization in the composite, from Equation 5-2, the relationship between the heat flux and temperature gradient is substituted to give

$$\langle \vec{p} \rangle = \langle \vec{q} \rangle - \underline{k}_2 \langle \vec{\nabla} T \rangle = \underline{k}_* \langle \vec{\nabla} T \rangle - \underline{k}_2 \langle \vec{\nabla} T \rangle = (\underline{k}_* - \underline{k}_2) \langle \vec{\nabla} T \rangle, \quad (5-3)$$

where $\langle \vec{p} \rangle$ is the volume average polarization in the composite, \underline{k}_* is the effective thermal conductivity in the composite, \underline{k}_2 is the thermal conductivity of the pure matrix (Vectra), and $\langle \vec{\nabla} T \rangle$ is the volume average temperature gradient in the composite. Since the polarization is zero in the matrix, the volume average polarization in the composite is given by $\langle \vec{p} \rangle = f_1 \langle \vec{p} \rangle_1$ where f_1 is the volume fraction of the filler and $\langle \vec{p} \rangle_1$ is the volume average polarization in the filler. Equation 5-3 simplifies to

$$\left(\underline{k}_* - \underline{k}_2\right) \langle \vec{\nabla} T \rangle = f_1 \langle \vec{p} \rangle_1. \quad (5-4)$$

Now the goal of this derivation is to find an expression for $\langle \vec{p} \rangle_1$ in terms of the volume average temperature gradient in the composite. To accomplish this the volume average polarization in the filler, $\langle \vec{p} \rangle_1$, is given as

$$\langle \vec{p} \rangle_1 = \left(\underline{k}_1 - \underline{k}_2\right) \langle \vec{\nabla} T \rangle_1, \quad (5-5)$$

and the volume average polarization in the filler is approximated from the inclusion problem as

$$\langle \vec{p} \rangle_1 = \langle \vec{p}_* \rangle_1 - \left(\underline{k}_2 - \underline{k}_*\right) \langle \vec{\nabla} T \rangle_1. \quad (5-6)$$

In Equations 5-5 and 5-6 $\langle \vec{\nabla} T \rangle_1$ is the volume average temperature gradient in the inclusion, $\langle \vec{p}_* \rangle_1$ is the volume average polarization in the inclusion relative to \underline{k}_* (from the inclusion problem), and \underline{k}_1 is the thermal conductivity of the inclusion. Solving Equations 5-5 and 5-6 for $\langle \vec{\nabla} T \rangle_1$ gives

$$\langle \vec{\nabla} T \rangle_1 = \left(\underline{k}_1 - \underline{k}_*\right)^{-1} \langle \vec{p}_* \rangle_1. \quad (5-7)$$

Now Equation 5-7 is substituted into Equation 5-5 to give

$$\langle \vec{p} \rangle_1 = \left(\underline{k}_1 - \underline{k}_2\right) \left(\underline{k}_1 - \underline{k}_*\right)^{-1} \langle \vec{p}_* \rangle_1. \quad (5-8)$$

The effective polarization in the filler relative to \underline{k}_* comes from the inclusion problem and is given by

$$\langle \vec{p}_* \rangle_1 = (\alpha V^{-1}) \underline{k}_* \langle \vec{\nabla} T \rangle, \quad (5-9)$$

where α is the thermal polarizability (defined below) of the ellipsoid (filler) with thermal conductivity \underline{k}_1 in a matrix of thermal conductivity \underline{k}_* and V is the volume of the inclusion. Substituting Equation 5-9 into Equation 5-8 results in

$$\langle \vec{p} \rangle_1 = \left(\underline{k}_1 - \underline{k}_* \right) \left(\underline{k}_1 - \underline{k}_* \right)^{-1} (\alpha V^{-1}) \underline{k}_* \langle \vec{\nabla} T \rangle. \quad (5-10)$$

The final step is to substitute Equation 5-10 into Equation 5-4 to give the expression for the effective thermal conductivity as

$$\underline{k}_* - \underline{k}_2 = f_1 \left\langle \left(\underline{k}_1 - \underline{k}_* \right) \left(\underline{k}_1 - \underline{k}_* \right)^{-1} (\alpha V^{-1}) \underline{k}_* \right\rangle. \quad (5-11)$$

In Equation 5-11 “< >” is a volume average over the entire polymer composite where as in Equations 5-6 through 5-10 “< >” dealt with volume average in a single inclusion. The polarizability, α , contains information on the geometry of the inclusion.

The geometry of the inclusion will be further defined here. In Figure 5.2-1, l'_i are the semi-axes of the anisotropic ellipsoidal inclusion. The semi-axes of the anisotropic ellipsoid are defined as

$$l'_1 = 1 \quad (5-12)$$

$$l'_2 = l'_3 = \frac{1}{AR} * l'_1, \quad (5-13)$$

where AR is the aspect ratio of the anisotropic ellipsoidal inclusion. Since the matrix (Vectra) is anisotropic a change of variables is used to transform the anisotropic matrix to an isotropic matrix so that the anisotropic inclusion is in a isotropic matrix phase. The transformation is given by

$$l_i = \frac{l'_i}{\sqrt{k_2[i,i]}} \quad \text{with } i = 1,2,3. \quad (5-14)$$

In the above equation $k_2[i,i]$ is the diagonal entry of the thermal conductivity of the matrix material.

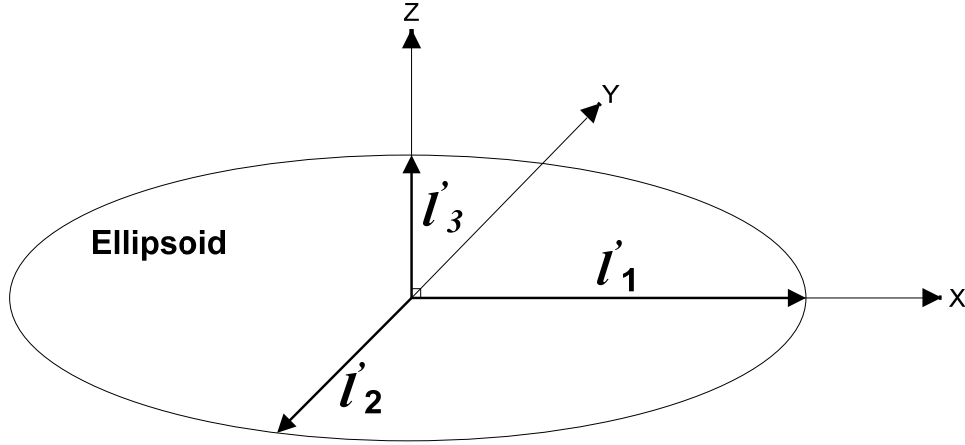


Figure 5.2-1: Diagram of Uncoated Ellipsoid (Synthetic Graphite and Carbon Black Models)

The last step in solving this inclusion problem is determining of the polarizability of the inclusion, α . The polarizability of the inclusion is given by Bohren and Huffman [8] as

$$\left(\underline{\underline{\alpha}}V^{-1}\right) = \left(\underline{\underline{k}}_1 - \underline{\underline{k}}_*\right) \left[\underline{\underline{k}}_* + \underline{\underline{D}} \left(\underline{\underline{k}}_1 - \underline{\underline{k}}_* \right) \right]^{-1}, \quad (5-15)$$

where $\underline{\underline{D}}$ is the depolarization tensor of the inclusion and is given as

$$\underline{\underline{D}} = \begin{pmatrix} d_1 & 0 & 0 \\ 0 & d_2 & 0 \\ 0 & 0 & d_3 \end{pmatrix}. \quad (5-16)$$

In Equation 5-16 d_1 , d_2 , and d_3 are the depolarization factors of the inclusion, and are given by

$$d_i(l_1, l_2, l_3) = \frac{l_1 l_2 l_3}{2} \int_0^\infty \frac{dy}{(l_i^2 + y) \sqrt{(l_1^2 + y)(l_2^2 + y)(l_3^2 + y)}} \text{ with } i = 1, 2, 3. \quad (5-17)$$

The integral in this equation is evaluated numerically in Mathematica. In summary, to compute \underline{k}_* Equations 5-15 to 5-17 are substituted into Equation 5-11, which gives rise to an implicit equation for \underline{k}_* . All of the given equations, Equations 5-11 and Equations 5-15 through 5-17, are evaluated in Mathematica. The Mathematica code for the synthetic graphite and carbon black model is in Appendix B.

5.2.2: Carbon Fiber Model

The coated ellipsoid assemblage model was first introduced by G.W. Milton [9], and this model is a generalization of the coated sphere assemblage model by Hashin and Shtrikman [10]. The basis of this model is when an appropriate effective thermal conductivity, \underline{k}_* , is chosen, a coated ellipsoid of thermal conductivity \underline{k}_1 with coating of the pure matrix at thermal conductivity \underline{k}_2 can be inserted as an inclusion in an infinite matrix material without disturbing the uniform temperature gradient outside the ellipsoid. Figure 5.2-2 depicts the inclusion problem. This type of inclusion problem has been solved by others such as Kerner, Benveniste and Miloh [11,12]. The coated ellipsoid assemblage model was used to predict the effective in-plane thermal conductivity for the carbon fiber/Vectra A950 polymer composite, because the surface of the carbon fiber was

treated with a proprietary binder to ensure adhesion with the polymer matrix (see Materials section of this paper).

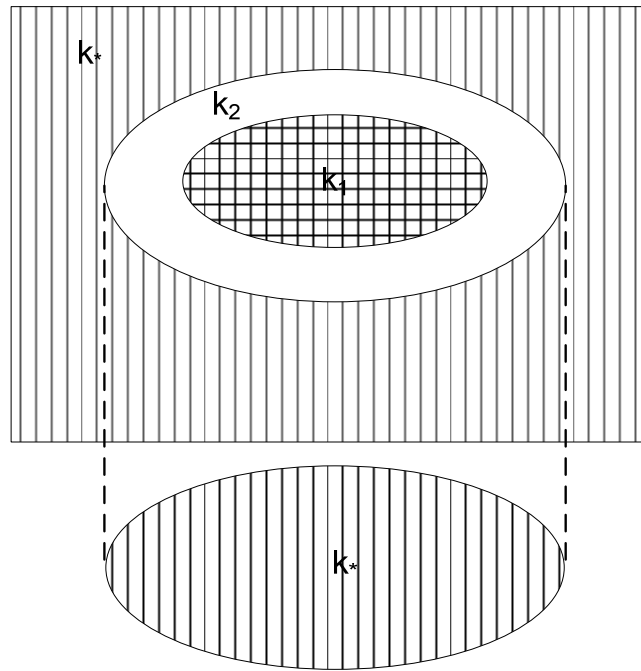


Figure 5.2-2: Diagram of Ellipsoidal Inclusion Problem (Carbon Fiber Model)

In this model there are two phases. The first phase contains the filler and the second phase contains the matrix material which acts as a coating on the filler. The first phase is embedded in the second phase, and the fillers are assumed to be ellipsoidal in shape and aligned in the horizontal plane of the composite. In this model, the thermal conductivity of the matrix and filler can be isotropic or anisotropic. Figure 5.2-3 shows a single coated ellipsoid.

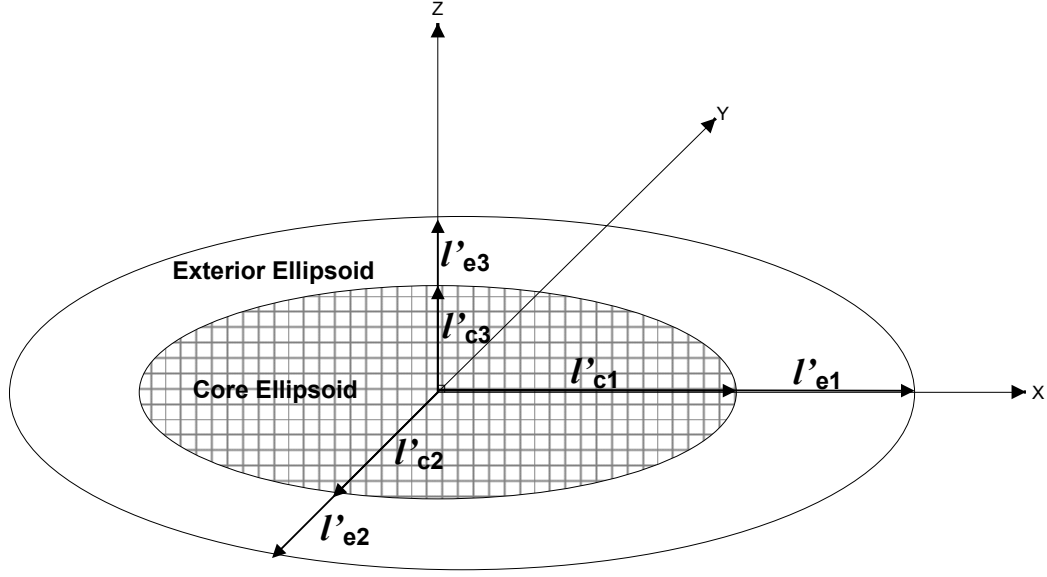


Figure 5.2-3: Diagram of Coated Ellipsoid (Carbon Fiber Model)

The effective in-plane thermal conductivity of the polymer composite is determined by the thermal conductivities of the filler and matrix, the volume fractions of the filler and matrix, and the geometry of the filler. The following equations are used to model the in-plane thermal conductivity of the carbon fiber/Vectra A950RX polymer composite and come from Milton's development [13]. The equation that predicts the effective thermal conductivity, $\underline{\underline{k}}_*$ (W/m·K) is given as

$$f_1 \left(\underline{\underline{k}}_* - \underline{\underline{k}}_2 \right)^{-1} = \left(\underline{\underline{k}}_1 - \underline{\underline{k}}_2 \right)^{-1} + (1 - f_1) \left(\underline{\underline{k}}_2 \right)^{-1/2} \underline{\underline{M}} \left(\underline{\underline{k}}_2 \right)^{-1/2}. \quad (5-18)$$

In this equation, $\underline{\underline{k}}_1$ (W/m·K) is the thermal conductivity of the filler, $\underline{\underline{k}}_2$ (W/m·K) is the thermal conductivity of the matrix, and f_1 is the filler volume fraction, and $\underline{\underline{M}}$ contains information on the geometry of the filler and is explained in more detail below.

Before introducing the equations that define $\underline{\underline{M}}$, the inclusion problem will be defined further. In Figure 5.2-3, l'_{ci} and l'_{ei} are the semi-axes of the anisotropic core and exterior ellipsoids of the inclusion. The semi-axes of the anisotropic core ellipsoid are defined in Equation 5-12 and 5-13 except with a “c” to denote core ellipsoid. Since the coating is anisotropic a change of variables is used to transform the inclusion problem. Transformation from the anisotropic exterior ellipsoid (matrix phase) to the isotropic exterior ellipsoid is given by Equation 5-14. The relationship between the anisotropic core ellipsoid and the isotropic exterior ellipsoid is

$$l_{ei} = \sqrt{l_{ci}^2 + \theta} \quad \text{with } i = 1, 2, 3 \quad (5-19)$$

where θ is a parameter determined by the volume fraction of the filler such that the following equation is satisfied

$$f_1 = \frac{l_{c1}l_{c2}l_{c3}}{l_{e1}l_{e2}l_{e3}}. \quad (5-20)$$

Now, with the inclusion problem defined, $\underline{\underline{M}}$ is computed by

$$\underline{\underline{M}} = (\underline{\underline{D}}_c - f_1 \underline{\underline{D}}_e) / (1 - f_1). \quad (5-21)$$

In this equation $\underline{\underline{D}}_c$ and $\underline{\underline{D}}_e$ are the depolarization tensors of the core and exterior ellipsoid, and f_1 is the volume fraction of the filler. The depolarization tensors are given in the following form

$$\underline{\underline{D}}_c = \begin{pmatrix} d_{c1} & 0 & 0 \\ 0 & d_{c2} & 0 \\ 0 & 0 & d_{c3} \end{pmatrix} \quad (5-22)$$

$$\underline{\underline{D_e}} = \begin{pmatrix} d_{e1} & 0 & 0 \\ 0 & d_{e2} & 0 \\ 0 & 0 & d_{e3} \end{pmatrix}, \quad (5-23)$$

where d_{ci} and d_{ei} are calculated numerically from the following formulas

$$d_{ci}(l_{c1}, l_{c2}, l_{c3}) = \frac{l_{c1}l_{c2}l_{c3}}{2} \int_0^\infty \frac{dy}{(l_{ci}^2 + y)\sqrt{(l_{c1}^2 + y)(l_{c2}^2 + y)(l_{c3}^2 + y)}} \text{ with } i = 1, 2, 3 \quad (5-24)$$

$$d_{ei}(l_{e1}, l_{e2}, l_{e3}) = \frac{l_{e1}l_{e2}l_{e3}}{2} \int_0^\infty \frac{dy}{(l_{ei}^2 + y)\sqrt{(l_{e1}^2 + y)(l_{e2}^2 + y)(l_{e3}^2 + y)}} \text{ with } i = 1, 2, 3. \quad (5-25)$$

In Equations 5-24 and 5-25, l_{ci} and l_{ei} are the semi-axis of the transformed coated ellipsoid defined above in Equation 5-14. To compute $\underline{\underline{k_*}}$, Equations 5-20 through 5-25 are substituted into Equation 5-18, which gives rise to an explicit equation for $\underline{\underline{k_*}}$. All of the given equations, Equations 5-18 and Equations 5-20 to 5-25, are evaluated in Mathematica. The Mathematica code for the carbon fiber model is in Appendix C.

5.3: RESULTS

5.3.1: Filler Length, Aspect Ratio, and Orientation Results

The length and aspect ratio of the Thermocarb synthetic graphite particles in the injection molded disks were typically 50 microns and 1.68, respectively. These values are similar to that of the as received material and prior work [14,15]. For the injection molded samples containing Fortafil 243, the length was typically 70 microns. The

corresponding fiber aspect ratio (length/diameter) was 9. These results agree with prior work [14-17].

Figures 5.3-1 and 5.3-2 display the orientation of the synthetic graphite particles and carbon fiber, respectively, in the injection molded disks. The synthetic graphite particles appear to be randomly oriented in the horizontal plane of the composite (particles lying in the plane). This is similar to the carbon fiber composite, Figure 5.3-2, where the carbon fibers all lie in the plane (though randomly oriented within this plane) as no circular fiber ends are present.

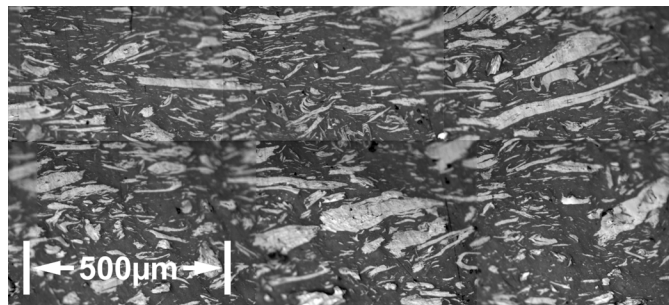


Figure 5.3-1: In-Plane Orientation for 40 wt% Synthetic Graphite in Vectra Injection Molded Disk at a Magnification of 200X

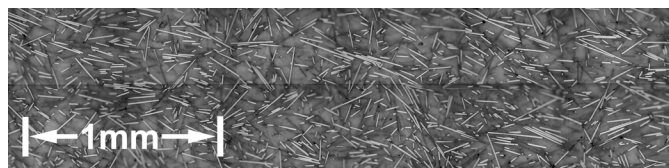


Figure 5.3-2: In-Plane Orientation for 20 wt% Carbon Fiber in Vectra Injection Molded Disk at a Magnification of 200X

5.3.2: In-Plane Thermal Conductivity Experimental Results

Figures 5.3-3 to 5.3-5 show the mean in-plane thermal conductivity results of the composites as a function of filler volume fraction for the synthetic graphite/Vectra composites, carbon black/Vectra composites, and carbon fiber/Vectra composites, respectively. These formulations correspond to that shown in Table 5.3-1. Figure 5.3-3 shows that the addition of synthetic graphite causes the in-plane thermal conductivity of the composite to increase from 1.00 W/m·K for Vectra to 4.33 W/m·K for composite containing 40 wt% SG (29.3 vol% SG) in Vectra. Figure 5.3-4 shows that the addition of carbon black causes the in-plane thermal conductivity of the composite to increase from 1.00 W/m·K for Vectra to 2.06 W/m·K for composite containing 15 wt% CB (12.1 vol% CB) in Vectra. Figure 5.3-5 shows that the addition of carbon fiber causes the in-plane thermal conductivity of the composite to increase from 1.00 W/m·K for Vectra to 2.49 W/m·K for composite containing 60 wt% CF (54.7 vol% CF) in Vectra. Adding synthetic graphite particles caused the largest increase in composite in-plane thermal conductivity.

Table 5.3-1: Single Filler Loading Levels in Vectra A950RX and Experimental and Model In-Plane Thermal Conductivity Results

Formulation	Filler wt %	Filler vol%	In-Plane Thermal Conductivity (W/m·K)	Predicted In-Plane Thermal Conductivity (W/m·K)
Vectra	0.0	0.0	1.00 ± 0.01 , n = 5	1.00
2.5CB	2.5	1.9	1.01 ± 0.01 , n = 5	1.10
4CB	4.0	3.1	1.05 ± 0.004 , n = 5	1.17
5CB	5.0	3.9	1.10 ± 0.01 , n = 5	1.22
6CB	6.0	4.7	1.22 ± 0.04 , n = 5	1.27
7.5CB	7.5	6.0	1.35 ± 0.02 , n = 5	1.37
10CB	10.0	8.0	1.62 ± 0.06 , n = 5	1.53
15CB	15.0	12.1	2.06 ± 0.08 , n = 5	1.95
10SG	10.0	6.5	1.42 ± 0.02 , n = 5	1.21
15SG	15.0	9.9	1.55 ± 0.03 , n = 5	1.37
20SG	20.0	13.5	1.96 ± 0.05 , n = 5	1.58
25SG	25.0	17.2	2.40 ± 0.03 , n = 5	1.87
30SG	30.0	21.1	2.83 ± 0.04 , n = 5	2.32
35SG	35.0	25.2	3.44 ± 0.05 , n = 5	3.08
40SG	40.0	29.3	4.33 ± 0.07 , n = 5	4.47
5CF	5.0	4.1	1.12 ± 0.02 , n = 5	1.22
7.5CF	7.5	6.1	1.18 ± 0.01 , n = 5	1.31
10CF	10.0	8.2	1.27 ± 0.02 , n = 5	1.40
15CF	15.0	12.4	1.41 ± 0.02 , n = 5	1.55
20CF	20.0	16.8	1.52 ± 0.02 , n = 5	1.69
25CF	25.0	21.2	1.62 ± 0.01 , n = 5	1.82
30CF	30.0	25.5	1.74 ± 0.04 , n = 5	1.93
35CF	35.0	30.2	1.87 ± 0.03 , n = 5	2.05
40CF	40.0	34.9	1.97 ± 0.02 , n = 5	2.17
45CF	45.0	39.7	2.09 ± 0.02 , n = 5	2.29
50CF	50.0	44.6	2.21 ± 0.03 , n = 5	2.41
55CF	55.0	49.6	2.31 ± 0.06 , n = 5	2.54
60CF	60.0	54.7	2.49 ± 0.03 , n = 5	2.68

5.3.3: In-Plane Thermal Conductivity Modeling Results

In the past our research group has used empirical parameter fitting to model the effective in-plane thermal conductivity of polymer composites [18]. In this work an assemblage of ellipsoidal inclusions model is used to model the effective in-plane thermal conductivity.

5.3.3.1 Synthetic Graphite Model

Using Equation 5-11 and Equations 5-15 through 5-17, the effective in-plane thermal conductivity of the synthetic graphite/Vectra A950RX composite was predicted. In Equation 5-11, “< >” denotes volume averaging for all horizontal rotations in the horizontal plane of the composite. The inputs for this model were $\underline{\underline{k_1}}$, $\underline{\underline{k_2}}$, AR , and f_l . The volume fraction f_l is obtained from the experimental data of the single filler formulations given in Table 5.3-1 for synthetic graphite, and ranged from 0.065 to 0.293. The AR was measured to be 1.7, and the input value of the thermal conductivity of the synthetic graphite (see Table 3.3-2), $\underline{\underline{k_1}}$ (W/m·K), is

$$\underline{\underline{k_1}} = \begin{bmatrix} 600 & 0 & 0 \\ 0 & 60 & 0 \\ 0 & 0 & 60 \end{bmatrix}. \quad (5-26)$$

The input value of the thermal conductivity of the Vectra A950RX polymer (matrix), $\underline{\underline{k_2}}$ (W/m·K), is

$$\underline{\underline{k_2}} = \begin{bmatrix} 1 & 0 & 0 \\ 0 & 1 & 0 \\ 0 & 0 & 0.22 \end{bmatrix}, \quad (5-27)$$

where 1 W/m²K is the thermal conductivity in the in-plane direction and 0.22 W/m²K is the thermal conductivity in the through-plane direction. These input values come directly from measurement of the pure Vectra A950RX polymer using the Hot Disk Thermal Constants Analyzer.

The results from modeling this polymer composite are given in Figure 5.3-3, where the diamonds are the experimental data and the curve is the model computed from Equation 5-11. This model shows good agreement with experimental data, and Table 5.3-1 shows the data predicted from the model.

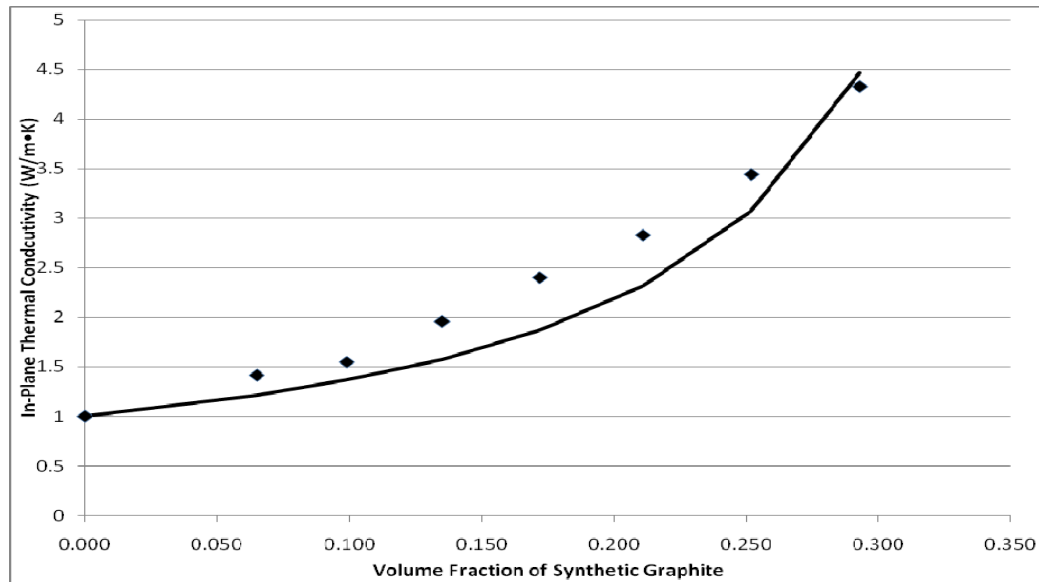


Figure 5.3-3: Modeling Results of In-Plane Thermal Conductivity of SG/Vectra Composites with Experimental Data Represented by Diamonds and Model Predictions (Equation 5-11) Represented by Curve

5.3.3.2 Carbon Black Model

Using Equation 5-11 and Equations 5-15 through 5-17 the effective in-plane thermal conductivity of the carbon black/Vectra A950RX composite was predicted. The inputs for this model were $\underline{k_1}$, $\underline{k_2}$, AR , and f_l . The volume fraction f_l was obtained from the experimental data of the single filler formulations given in Table 5.3-1 for carbon black, and range from 0.019 to 0.121. The input value of the thermal conductivity of the Vectra A950RX polymer, $\underline{k_2}$ (W/m·K), is the same as shown in Equation 5-27.

The AR and $\underline{k_1}$ could not be measured directly for carbon black due to the small size of the particle, thus these values were estimated. The AR was estimated to be 5 because carbon black easily separates into aggregates when mixed with polymer. To estimate values for the axial and non-axial direction thermal conductivity the experimental data for the carbon black/Vectra and carbon fiber/Vectra were compared. At equal volume fractions the measured in-plane thermal conductivity of carbon black/Vectra was higher than the carbon fiber/Vectra composite. This can be seen in Table 5.3-1 at 12.1 vol% of carbon black and 12.4 vol % of carbon fiber the in-plane thermal conductivity was measured to be 2.06 W/m·K and 1.41 W/m·K, respectively. Therefore, $\underline{k_1}$ (W/m·K) for carbon black was estimated to be slightly higher than that of the carbon fiber and is given as

$$\underline{k_1} = \begin{bmatrix} 30 & 0 & 0 \\ 0 & 30 & 0 \\ 0 & 0 & 30 \end{bmatrix}. \quad (5-28)$$

The results from the modeling are given in Figure 5.3-4, where the diamonds are the experimental data and the curve is predicted by Equation 5-11. At low volume fractions this model overestimates the experimental data and at higher volume fractions the model underestimates the experimental data. This result may come from the aspect ratio being estimated as 5 for all volume fractions. As the volume fraction increases carbon black may be forming chains inside the composite which means at higher volume fractions the aspect ratio may be higher. This model shows good agreement with experimental data, and Table 5.3-1 shows the data predicted from the model.

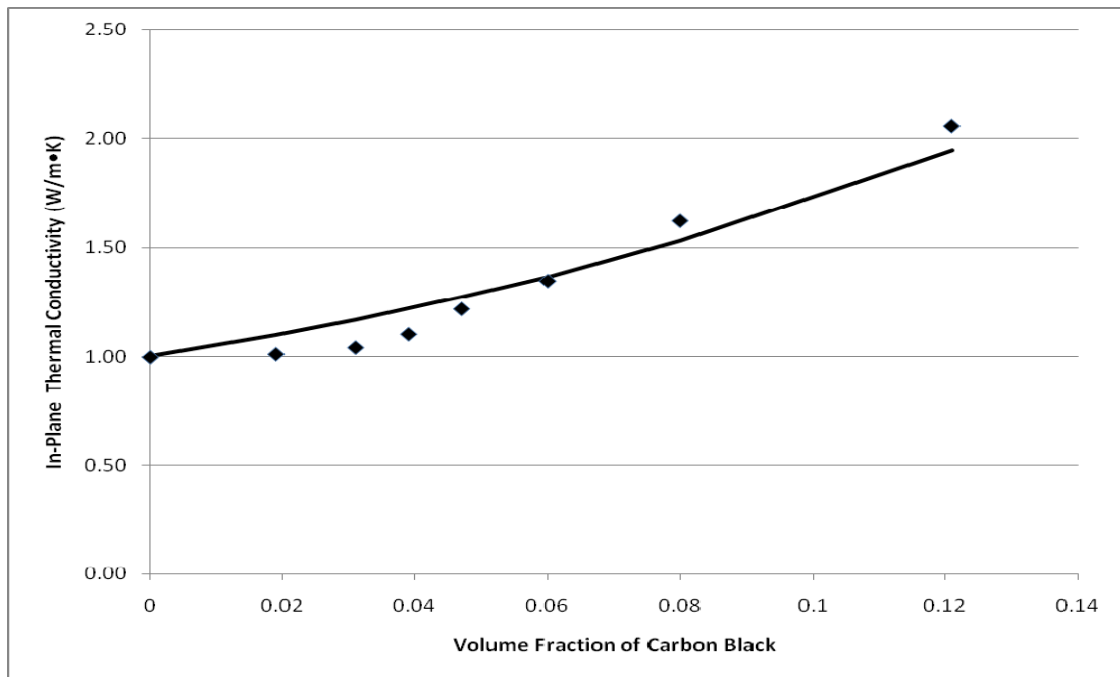


Figure 5.3-4: Modeling Results of In-Plane Thermal Conductivity of CB/Vectra Composites with Experimental Data Represented by Diamonds and Model Predictions (Equation 5-11) Represented by Curve

5.3.3.3: Carbon Fiber Model

Using Equation 5-18 and Equations 5-20 through 5-25, the effective in-plane thermal conductivity of the carbon fiber/Vectra A950RX composite was modeled. The form of Equation 5-18 that was used to compute the effective in-plane thermal conductivity was

$$\underline{\underline{k}}_* = f_1 \left[\left(\underline{\underline{k}}_1 - \underline{\underline{k}}_2 \right)^{-1} + (1 - f_1) \left(\underline{\underline{k}}_2 \right)^{-1/2} \underline{\underline{M}} \left(\underline{\underline{k}}_2 \right)^{-1/2} \right]^{-1} + \underline{\underline{k}}_2. \quad (5-29)$$

The inputs to the model were $\underline{\underline{k}}_1$, $\underline{\underline{k}}_2$, AR , and f_1 . The volume fraction f_1 is obtained from the experimental data of the single filler formulations given in Table 5.3-1 for carbon fiber, and range from 0.041 to 0.547. The AR was measured to be 9, and the input value of the thermal conductivity of the carbon fiber (see Table 3.3-3), $\underline{\underline{k}}_1$ (W/m²K), is

$$\underline{\underline{k}}_1 = \begin{bmatrix} 20 & 0 & 0 \\ 0 & 2.5 & 0 \\ 0 & 0 & 2.5 \end{bmatrix}. \quad (5-30)$$

The input value of the thermal conductivity of the Vectra A950RX polymer, $\underline{\underline{k}}_2$ (W/m²K), is the same as Equation 5-27. Since the assumption is made that the coated ellipsoids are aligned, the tensors $\underline{\underline{k}}_1$ and $\underline{\underline{k}}_2$ only have non-zero entries on the diagonal.

Therefore, calculating $\left(\underline{\underline{k}}_2 \right)^{-1/2}$ from Equation 5-29 is done by taking the square root of each diagonal entry and then inverting the matrix. To determine the effective in-plane thermal conductivity from $\underline{\underline{k}}_*$ the harmonic mean was used. For example, when the volume fraction of carbon fiber is 0.547 $\underline{\underline{k}}_*$ is given by

$$\underline{k_*} = \begin{bmatrix} 10.2 & 0 & 0 \\ 0 & 1.54 & 0 \\ 0 & 0 & 0.82 \end{bmatrix}. \quad (5-31)$$

The harmonic mean, H , used to average entry $k_*[1,1]$ and $k_*[2,2]$, is computed by

$$H = \frac{2 * k_*[1,1] k_*[2,2]}{k_*[1,1] + k_*[2,2]}, \quad (5-32)$$

to give an effective in-plane thermal conductivity 2.68 W/mK and this can be seen in Figure 5.3-5.

The results from modeling this polymer composite are given in Figure 5.3-5, where the diamonds are the experimental data and the curve is the model. This model overestimates the experimental data because the carbon fibers were assumed to be aligned in the composite. Some of the carbon fiber particles in the actual polymer composite may be slightly tilted away from the direction in which the in-plane thermal conductivity is measured, slightly reducing the overall in-plane thermal conductivity. This model shows good agreement with experimental data, and Table 5.3-1 shows the data predicted from the model by Equation 5-29.

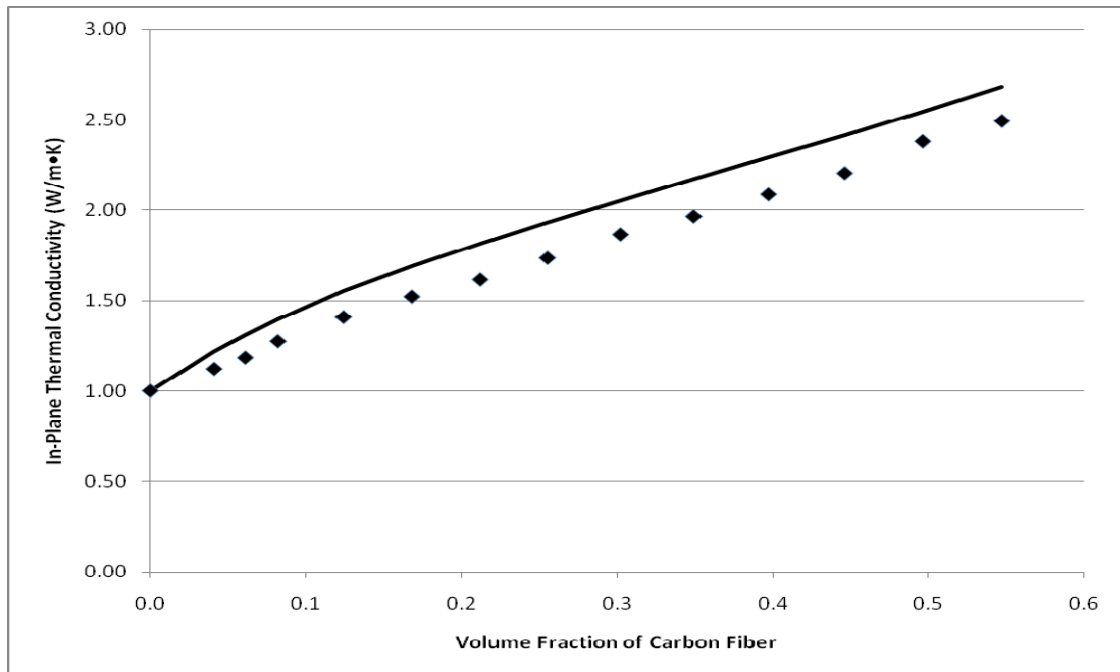


Figure 5.3-5: Modeling Results of In-Plane Thermal Conductivity of CF/Vectra Composites with Experimental Data Represented by Diamonds and Model Predictions (Equation 5-22) Represented by Curve

5.4: CONCLUSIONS

The objectives of this research were to measure in-plane thermal conductivity and develop models to predict the effective in-plane thermal conductivity for composites containing varying amounts of a single filler (either carbon black, synthetic graphite, or carbon fiber) in Vectra. In previous work by R.A. Hauser [18] effective in-plane thermal conductivity models had been developed by parameter fitting. In this work, the models developed used only physical properties of the composite material constituents, geometry, and information on the processing. From Hauser's work, the synthetic graphite

filler caused the greatest increase in the effective in-plane thermal conductivity of the composites.

Two models were used to derive expressions to predict the effective in-plane thermal conductivity of the polymer composites. An uncoated ellipsoid inclusion problem was used to model the effective in-plane thermal conductivity of the synthetic graphite and carbon black/Vectra polymer composites. This model used the polarization field in the average field approximation to predict the effective in-plane thermal conductivity. As we have shown, this model can be utilized for isotropic or anisotropic filler and matrix materials, and provided good agreement with the experimental data.

The second model used a coated ellipsoid inclusion problem to model the effective in-plane thermal conductivity of the carbon fiber/Vectra polymer composite. This model used the temperature gradient and heat flux in the inclusion problem to predict the effective in-plane thermal conductivities of the polymer composite. This model can be utilized for isotropic or anisotropic filler and matrix materials, and gave good agreement with experimental data. Developing these models are of interest because having a model that can predict the effective in-plane thermal conductivity of polymer composites from known physical properties of its constituents can reduce experimental work and save time and money.

5.5: REFERENCES

1. R. B. Bird, W.E. Stewart and E.N. Lightfoot, *Transport Phenomena*, 2nd edition, John Wiley & Son, Inc, New York (2001).
2. D. Polder and J.H. Van Santen, *Physica*, **12**, 257 (1946).
3. G.W. Milton, *Communications in Mathematical Physics*, **99**, 463 (1985).
4. J. Helsing and A. Helte, *Journal of Applied Physics*, **69**, 3583 (1991).
5. S. Kirkpatrick, *Reviews of Modern Physics*, **45**, 574 (1973).
6. T.W. Noh, *Physical Review B – Solid State*, **44**, 5459 (1991).
7. D. Stroud, *Physical Review B – Solid State*, **12**, 3368 (1975).
8. C.F. Bohren and D.R. Huffman, *Absorption and Scattering of Light by Small Particles*, John Wiley & Sons, Inc, (1983).
9. G.W. Milton, *Applied Physics Letters*, **37**, 300 (1980).
10. Z. Hashin and S. Shtrikman, *Journal of Applied Physics*, **33**, 3125 (1962).
11. E.H. Kerner, *Proceedings of the Physical Society*, **69**, 808 (1956).
12. Y. Benveniste and T. Miloh, *Journal of Mechanics and Physics of Solids*, **47**, 1873 (1999).
13. G.W. Milton, *The Theory of Composites*, Cambridge University Press, New York (2002).
14. J.A. Heiser, J.A. King, J.P. Konell, and L.L. Sutter, *Polymer Composites*, **25**, 407 (2004).
15. J.P. Konell, J.A. King, and I. Miskioglu, *Polymer Composites*, **25**, 172 (2004).
16. J.A. Heiser and J.A. King, *Polymer Composites*, **25**, 186 (2004).

17. E.H. Weber, M.L. Clingerman, and J.A. King, *Journal of Applied Polymer Science*, **88**, 123 (2003).
18. R.A. Hauser, J.M. Keith, J.A. King, and J.L. Holdren, *Journal of Applied Polymer Science*, **100**, 2914 (2008).

Chapter 6: Summary, Conclusions, and Future Work

6.1: Summary

Different concentrations of Ketjenblack EC-600 JD carbon black, Thermocarb TC-300 synthetic graphite, and Fortafil 243 carbon fiber were added to Vectra A950RX. The maximum single filler content studied were 15 wt% for carbon black, 40 wt% for synthetic graphite, and 60 wt% for carbon fiber. The in-plane thermal conductivity of each composite formulation was measured using the transient plane source technique at 23°C. Two different models were used to model the effective in-plane thermal of each composite formulations. An uncoated ellipsoid inclusion problem was used to predict the effective in-plane thermal conductivity of the composites containing carbon black and synthetic graphite. A coated ellipsoid inclusion problem was used to predict the effective in-plane thermal conductivity of the composite containing carbon fiber.

For the composites containing carbon black, at the highest filler level (15 wt %), the composite effective in-plane thermal conductivity increased from 0.99 W/m·K (neat Vectra) to 2.06 W/m·K, and the predicted effective in-plane thermal conductivity was 1.95 W/m·K. For the composites containing Thermocarb TC-300 synthetic graphite, at the highest filler level (40 wt %), the composites effective in-plane thermal conductivity increases from 0.99 W/m·K (neat Vectra) to 4.33 W/m·K, and the predicted effective in-plane thermal conductivity was 4.47 W/m·K. For the composites containing Fortafil 243 carbon fiber, at the highest filler level (60 wt %), the effective in-plane thermal

conductivity increased from 0.99 W/m·K (neat Vectra) to 2.49 W/m·K, and the predicted effective in-plane thermal conductivity was 2.68 W/m·K. The percent error between the measured and predicted effective in-plane thermal conductivity was 5%, 3%, and 8% for carbon black, synthetic graphite and carbon fiber, respectively. The Thermocarb TC-300 synthetic graphite caused the greatest increase in the effective in-plane thermal conductivity of the composite.

6.2: Conclusions

The objectives of this research were to measure in-plane thermal conductivity and develop models to predict the effective in-plane thermal conductivity for composites containing varying amounts of a single filler (either carbon black, synthetic graphite, or carbon fiber) in Vectra. In previous modeling work by R.A. Hauser [1], effective in-plane thermal conductivity models had been developed by parameter fitting. In this work, the models developed used only physical properties of the composite material constituents, geometry, and information on the processing.

Two models were used to derive expressions to predict the effective in-plane thermal conductivity of the polymer composites. An uncoated ellipsoid inclusion problem was used to model the effective in-plane thermal conductivity of the synthetic graphite and carbon black/Vectra polymer composites. This model used the polarization field in the average field approximation to predict the effective in-plane thermal conductivity.

This model can be utilized for isotropic or anisotropic filler and matrix materials, and provided good agreement with the experimental data.

The second model used a coated ellipsoid inclusion problem to model the effective in-plane thermal conductivity of the carbon fiber/Vectra polymer composite. This model used the temperature gradient and heat flux in the inclusion problem to predict the effective in-plane thermal conductivities of the polymer composite. This model can be utilized for isotropic or anisotropic filler and matrix materials, and gave good agreement with experimental data. Developing these models are of interest because having a model that can predict the effective in-plane thermal conductivity of polymer composites from known physical properties of its constituents can reduce experimental work and save time and money.

6.3: Recommendations for Future Work

This study focused on predicting the in-plane thermal conductivity for composites containing either carbon black, synthetic graphite, or carbon fiber. Each of these fillers increased the in-plane thermal conductivity of the composite, and this was easily shown by the models used. Useful applications of these composite materials are in heat sink applications and in bipolar plates for fuel cells.

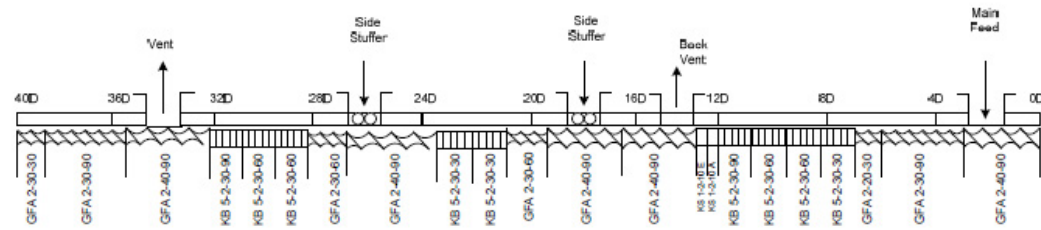
This work showed that synthetic graphite caused the largest increase in composite in-plane thermal conductivity when added to Vectra A950RX LCP. In Hauser's work,

single filler and multiple filler composites were made and modeled using Nielsen's model. For future work, a model should be developed that can predict the in-plane thermal conductivity of a composite with multiple fillers using information about the physical properties of constituents, geometry and processing. Also, in Hauser's work the through-plane thermal conductivity was measured and modeled using parameter fitting. So for future work, a model should be developed that can predict the through-plane thermal conductivity for composites containing single and multiple fillers using information about the physical properties of the constituents, geometry, and processing.

6.4: References

1. Hauser, R. A., “Synergistic Effects and Modeling of Thermally Conductive Resins for Fuel Cell Bipolar Plate Applications”, Ph.D. Dissertation, Michigan Technological University, Houghton, MI, 2008.

Appendix A: Extruder Screw Design



For Screw Type Elements

GFA-d-ee-ff
 G = co-rotating
 F = conveying
 A = Free-Meshing
 d = number of threads
 ee = pitch (length in millimeters for one complete rotation)
 ff = length of screw elements in millimeters

Kneading disks

KBj-d-kk-l
 KB = kneading block
 j = number of kneading segments
 d = number of threads
 k = length of kneading block in millimeters
 l = twisting angle of the individual kneading segments

Kneading disks

KS1-d-hh-i
 KS1 = Kneading disc
 d = number of threads
 h = length of kneading disc in millimeters
 i = A for initial disc and E for end disc

Zones

0D to 4D is Zone 1 (water cooled, not heated)
 4D to 8D is Zone 2 and Heating Zone 1
 8D to 12D is Zone 3 and Heating Zone 2
 12D to 16D is Zone 4 and Heating Zone 3
 16D to 20D is Zone 5 and Heating Zone 4
 20D to 24D is Zone 6 and Heating Zone 5
 24D to 28D is Zone 7 and Heating Zone 6
 28D to 32D is Zone 8 and Heating Zone 7
 32D to 36D is Zone 9 and Heating Zone 8
 36D to 40D is Zone 10 and Heating Zone 9
 Nozzle is Heating Zone 10

Figure A.1: Extruder Screw Design

Appendix B : Mathematica Code for Synthetic Graphite and Carbon Black Models

```

Transversely isotropic (averaging over horizontal rotations);

(*Average polarization approximation,
using the polarization p = j - km(grad T)
as in Milton, p.199
*)
Clear[ki, km, kstar, a, b, c, diag, asp, f1];

diag[{a_, b_, c_}] = {{a, 0, 0}, {0, b, 0}, {0, 0, c}};

(* Enter conductivities for inclusions and matrix *)
Clear[KPtran, ki, km, f1, asp];
KPtran[ki_, km_, f1_, asp_] :=
Module[{l1prime, l2prime, l3prime, l1, l2, l3,
  fun1, fun2, fun3, d1, d2, d3, kstar, y, alph1, alph2, alph3,
  rhs1, rhs2, rhs3, fred, ethel, first, third, kstar1, kstar3},
If[km[[1]] ≠ km[[2]], Print["ERROR! km must be transversely isotropic"]];
l1prime = 1;
l2prime = l1prime * asp;
l3prime = l2prime;
l1 = l1prime / Sqrt[km[[1]]];
l2 = l2prime / Sqrt[km[[2]]];
l3 = l3prime / Sqrt[km[[3]]];
fun1 =
  l1 * l2 * l3 / 2 * 1 / ( (l1^2 + y) * Sqrt[(l1^2 + y) * (l2^2 + y) * (l3^2 + y)] );
fun2 = l1 * l2 * l3 / 2 * 1 / ( (l2^2 + y) * Sqrt[(l1^2 + y) * (l2^2 + y) * (l3^2 + y)] );
fun3 = l1 * l2 * l3 / 2 *
  1 / ( (l3^2 + y) * Sqrt[(l1^2 + y) * (l2^2 + y) * (l3^2 + y)] );
Clear[d1, d2, d3, y];
d1 = NIntegrate[fun1, {y, 0, Infinity}];
d2 = NIntegrate[fun2, {y, 0, Infinity}];
d3 = NIntegrate[fun3, {y, 0, Infinity}];
If[Abs[d1 + d2 + d3 - 1] > 10^(-5), Print["ERROR: problem with d1,d2,d3"]];
Clear[alph1, alph2, alph3, kstar, kstar1, kstar3];
kstar = {kstar1, kstar1, kstar3};
alph1 = (ki[[1]] - kstar[[1]]) / (kstar[[1]] + d1 * (ki[[1]] - kstar[[1]]));
alph2 = (ki[[2]] - kstar[[2]]) / (kstar[[2]] + d2 * (ki[[2]] - kstar[[2]]));
alph3 = (ki[[3]] - kstar[[3]]) / (kstar[[3]] + d3 * (ki[[3]] - kstar[[3]]));
Clear[rhs1, rhs2, rhs3, fred, ethel, first, third];
rhs1 = (ki[[1]] - km[[1]]) * (ki[[1]] - kstar[[1]])^(-1) * alph1 * kstar[[1]];
rhs2 = (ki[[2]] - km[[2]]) * (ki[[2]] - kstar[[2]])^(-1) * alph2 * kstar[[2]];
rhs3 =
  (ki[[3]] - km[[3]]) * (ki[[3]] - kstar[[3]])^(-1) * alph3 * kstar[[3]]; fred =
  FindRoot[kstar[[1]] - km[[1]] == f1 * 1 / 2 * (rhs1 + rhs2), {kstar1, ki[[1]]}];
ethel = FindRoot[kstar3 - km[[3]] == f1 * rhs3, {kstar3, ki[[3]]}];
first = kstar1 /. fred;
third = kstar3 /. ethel;
diag[{first, first, third}]

```

```
MatrixForm[KPtran[{600, 60, 60}, {1, 1, .22}, 0.065, 1 / 1.7]]
```

$$\begin{pmatrix} 1.09864 & 0 & 0 \\ 0 & 1.09864 & 0 \\ 0 & 0 & 0.235485 \end{pmatrix}$$

Appendix C: Mathematica Code for Carbon Fiber Model

Aligned Coated Ellipsoids Model

Anisotropic Constituents

(from Milton, "The Theory of Composites", 2002, pp.124-129 and pp.148-149)

Core/particle is material "1" and matrix is material "2".

Ellipsoids are axisymmetric about X_1 .

ellipsoids: $asp < 1 \Rightarrow$ torpedos

"alpha" determines f_1 : $f_1 = 1$ if $\alpha = 0$; $f_1 = 0$ if $\alpha = \infty$.

"kstar" determines effective conductivity as a function of

1. "k1" - the conductivity of the anisotropic particles
2. "k2" - the conductivity of the anisotropic matrix
3. "asp" - the aspect ratio of the ellipsoids: l_2/l_1
4. "alpha" - determines the volume fraction of f_1 ($0 < \alpha < \infty \Leftrightarrow 1 > f_1 > 0$)

```
$Assumptions = {k1 > 0, k2 > 0, 0 < f1 < 1};
$Assumptions = {a > 0, b > 0, c > 0, d > 0, e > 0};
$Assumptions = {alpha > 0, asp > 0};
$Assumptions = {lc1 > 0, lc2 > 0, lc3 > 0};
$Assumptions = {le1 > 0, le2 > 0, le3 > 0};

Clear[k1, k2, f1, M, kstar]
Clear[a, b, c, d, e]

(*Define the known values of the core semiaxis
(carbon filler) based on the aspect ratio of the carbon filler*)
Clear[lc1, lc2, lc3]
lc1prime[asp_] := 1
lc2prime[asp_] := asp * lc1prime[asp];
lc3prime[asp_] := lc2prime[asp];

lc1[asp_, c_] := lc1prime[asp] / Sqrt[c];
lc2[asp_, d_] := lc2prime[asp] / Sqrt[d];
lc3[asp_, e_] := lc3prime[asp] / Sqrt[e];

(*Computing the semi-axis of the exterior ellipsoid Eqn 7.56*)
Clear[le1, le2, le3]
le1[asp_, alpha_, c_] := Sqrt[lc1[asp, c]^2 + alpha];
le2[asp_, alpha_, d_] := Sqrt[lc2[asp, d]^2 + alpha];
le3[asp_, alpha_, e_] := Sqrt[lc3[asp, e]^2 + alpha];
```

```

(*calculation of the volume fraction f1 of the carbon filler as
a function based on the core and exterior semiaxis Eqn 7.51*)
Clear[f1]
f1[asp_, alpha_, c_, d_, e_] := lc1[asp, c] * lc2[asp, d] *
lc3[asp, e] / (lc1[asp, alpha, c] * lc2[asp, alpha, d] * lc3[asp, alpha, e]);

Clear[dc1, dc2, dc3]
dc1[asp_, c_, d_, e_] :=
((lc1[asp, c] * lc2[asp, d] * lc3[asp, e]) / 2) * NIntegrate[
1 / ((lc1[asp, c]^2 + y) * Sqrt[(lc1[asp, c]^2 + y) * (lc2[asp, d]^2 + y) *
(lc3[asp, e]^2 + y)]), {y, 0, Infinity}];
dc2[asp_, c_, d_, e_] := ((lc1[asp, c] * lc2[asp, d] * lc3[asp, e]) / 2) *
NIntegrate[1 / ((lc2[asp, d]^2 + y) * Sqrt[(lc1[asp, c]^2 + y) *
(lc2[asp, d]^2 + y) * (lc3[asp, e]^2 + y)]), {y, 0, Infinity}];
dc3[asp_, c_, d_, e_] := ((lc1[asp, c] * lc2[asp, d] * lc3[asp, e]) / 2) *
NIntegrate[1 / ((lc3[asp, e]^2 + y) * Sqrt[(lc1[asp, c]^2 + y) *
(lc2[asp, d]^2 + y) * (lc3[asp, e]^2 + y)]), {y, 0, Infinity}];

Clear[de1, de2, de3]
de1[asp_, alpha_, c_, d_, e_] :=
((lc1[asp, alpha, c] * lc2[asp, alpha, d] * lc3[asp, alpha, e]) / 2) *
NIntegrate[1 / ((lc1[asp, alpha, c]^2 + y) *
Sqrt[(lc1[asp, alpha, c]^2 + y) * (lc2[asp, alpha, d]^2 + y) *
(lc3[asp, alpha, e]^2 + y)]), {y, 0, Infinity}];
de2[asp_, alpha_, c_, d_, e_] := ((lc1[asp, alpha, c] * lc2[asp, alpha, d] *
lc3[asp, alpha, e]) / 2) * NIntegrate[1 / ((lc2[asp, alpha, d]^2 + y) *
Sqrt[(lc1[asp, alpha, c]^2 + y) * (lc2[asp, alpha, d]^2 + y) *
(lc3[asp, alpha, e]^2 + y)]), {y, 0, Infinity}];
de3[asp_, alpha_, c_, d_, e_] := ((lc1[asp, alpha, c] * lc2[asp, alpha, d] *
lc3[asp, alpha, e]) / 2) * NIntegrate[1 / ((lc3[asp, alpha, e]^2 + y) *
Sqrt[(lc1[asp, alpha, c]^2 + y) * (lc2[asp, alpha, d]^2 + y) *
(lc3[asp, alpha, e]^2 + y)]), {y, 0, Infinity}];

Clear[Dc, De]
Dc[asp_, c_, d_, e_] := {{dc1[asp, c, d, e], 0, 0},
{0, dc2[asp, c, d, e], 0}, {0, 0, dc3[asp, c, d, e]}};
De[asp_, alpha_, c_, d_, e_] := {{de1[asp, alpha, c, d, e], 0, 0},
{0, de2[asp, alpha, c, d, e], 0}, {0, 0, de3[asp, alpha, c, d, e]}};

Clear[M]
M[asp_, alpha_, c_, d_, e_] :=
(Dc[asp, c, d, e] - f1[asp, alpha, c, d, e] * De[asp, alpha, c, d, e]) /
(1 - f1[asp, alpha, c, d, e]);

Clear[k1, k2, kstar]
k1[a_, b_] := {{a, 0, 0}, {0, b, 0}, {0, 0, b}}; (*carbon filler*)
k2[c_, d_, e_] := {{c, 0, 0}, {0, d, 0}, {0, 0, e}}; (*polymer matrix*)
kstar[k1_, k2_, asp_, alpha_, c_, d_, e_] :=
Inverse[Inverse[k1 - k2] / f1[asp, alpha, c, d, e] +
((1 - f1[asp, alpha, c, d, e]) / f1[asp, alpha, c, d, e]) *
Inverse[Sqrt[k2]]].M[asp, alpha, c, d, e].Inverse[Sqrt[k2]] + k2;

```

```

(*****
*****
*****
(*Summary of Results From Given Inputs*)
Clear[a, b, c, d, e, asp, alpha];
a = 20; (* Thermal conductivity for carbon filler axial direction *)
b = 2.5; (* Thermal conductivity for carbon
filler in axis perpendicular to axial direction *)
c = 1; (* Thermal conductivity of the polymer matrix in axial direction*)
d = 1; (* Thermal conductivity of the polymer in the non-axial direction*)
e = 0.22;
(* Thermal conductivity of the polymer in the non-axial direction*)

asp = 1/9; (* Aspect ratio for carbon filler *)
alpha = 0.491; (* "Alpha" as defined above
to compute volume fraction for carbon filler*)

(* Check to see Equation 8.18 is satisfied*)
Clear[Lc, Le, Lcprime, Leprime1, Leprime2]
Lc := {{lc1[asp, c]^2, 0, 0}, {0, lc2[asp, d]^2, 0}, {0, 0, lc3[asp, e]^2}};
Le := {{le1[asp, alpha, c]^2, 0, 0},
{0, le2[asp, alpha, d]^2, 0}, {0, 0, le3[asp, alpha, e]^2}};
Lcprime := k2[c, d, e]^(1/2).Lc.k2[c, d, e]^(1/2);
Leprime1 := Lcprime + alpha*k2[c, d, e];
Leprime2 := Sqrt[k2[c, d, e]]*Le*Sqrt[k2[c, d, e]];

Print["Summary of inputs and outputs"];
Print[" "];
Print["k*=", MatrixForm[kstar[k1[a, b], k2[c, d, e], asp, alpha, c, d, e]]];
Print["k_particle=", MatrixForm[k1[a, b]], " ", "k_matrix=",
MatrixForm[k2[c, d, e]], " ", "aspect ratio l2/l1=", asp,
" ", "f1=", f1[asp, alpha, c, d, e], " ", "alpha=", alpha];
Print[""];

Print["This is a check to see if conditions are satisfied"];
Print[""];
Print["Leprime1 and Leprime2 must
equal so that equation 8.18 on p.148 is satisfied"];
Print[""];
Print["Leprime1=", MatrixForm[Leprime1]];
Print["Leprime2=", MatrixForm[Leprime2]];
(*****
*****

```

Summary of inputs and outputs

$$k^* = \begin{pmatrix} 1.48794 & 0. & 0. \\ 0. & 1.03139 & 0. \\ 0. & 0. & 0.243659 \end{pmatrix}$$

$$k_{\text{particle}} = \begin{pmatrix} 20 & 0 & 0 \\ 0 & 2.5 & 0 \\ 0 & 0 & 2.5 \end{pmatrix} \quad k_{\text{matrix}} = \begin{pmatrix} 1 & 0 & 0 \\ 0 & 1 & 0 \\ 0 & 0 & 0.22 \end{pmatrix}$$

$$\text{aspect ratio } l_2/l_1 = \frac{1}{9} \quad f_1 = 0.0410763 \quad \alpha = 0.491$$

This is a check to see if conditions are satisfied

Leprime1 and Leprime2 must equal so that equation 8.18 on p.148 is satisfied

$$\text{Leprime1} = \begin{pmatrix} 1.491 & 0. & 0. \\ 0. & 0.503346 & 0. \\ 0. & 0. & 0.120366 \end{pmatrix}$$

$$\text{Leprime2} = \begin{pmatrix} 1.491 & 0 & 0 \\ 0 & 0.503346 & 0 \\ 0 & 0 & 0.120366 \end{pmatrix}$$

Appendix D: Permission Letter

From: "Rebecca Wroblewski" <Rebecca.Wroblewski@UOP.com>
To: "Tayloria Adams" <tnadams@mtu.edu>
Cc: "Julia King" <jaking@mtu.edu>
Sent: Wednesday, December 15, 2010 9:43:36 AM GMT -05:00 US/Canada Eastern
Subject: RE: SEM photos

Tayloria,
Yes, you have my permission to use the requested images from my dissertation.

Regards,
Becca

Rebecca A. Wroblewski
Hydroprocessing R&D
UOP LLC - A Honeywell Company
8400 Joliet Road
McCook, IL 60525
Office: (708) 442.3865 (B34-R248)
Cell: (630) 310.7573
Email: Rebecca.Wroblewski@uop.com

From: Tayloria Adams [mailto:tnadams@mtu.edu]
Sent: Tuesday, December 14, 2010 10:05 PM
To: Wroblewski, Rebecca
Cc: Julia King
Subject: Re: SEM photos

Hello Becca,

The figures that I would like to use in my thesis from your dissertation are:

Figure 3.3-1 Carbon Black Aggregate
Figure 3.3-2 Thermocarb TC-300 Synthetic Graphite ESEM Image at 200x Magnification
Figure 3.3-6 Fortafil 243 Carbon Fiber ESEM Image at 250x Magnification
Figure 3.3-7 Fortafil 243 Carbon Fiber ESEM Image at 10000x Magnification
-Tayloria